Interplay Between FoxM1 and Dab2 Promotes Endothelial Cell Responses in Diabetic Wound Healing

Sudarshan Bhattacharjee[1,2], Jianing Gao[1,2], Yao Wei Lu[1,2#], Shahram Eisa-Beygi[1,2], Hao Wu[1,2], Kathryn Li[1], Amy E. Birsner[1,3], Scott Wong [1,2], Yudong Song[4], John Y-J. Shyy[5], Douglas B. Cowan[1,2], Wenyi Wei[6], Masanori Aikawa[7], Jinjun Shi[4], Hong Chen[1,2]*

[1] Vascular Biology Program, Boston Children's Hospital, Boston, MA 02115, USA

[2] Department of Surgery, Harvard Medical School, Boston, MA 02115, USA

[3] Department of Ophthalmology, Harvard Medical School, Boston, MA 02115, USA

[4] Center for Nanomedicine and Department of Anesthesiology, Perioperative and Pain Medicine, Brigham and Women's Hospital, Harvard Medical School, Boston, MA 02115, USA

[5] Division of Cardiovascular Medicine, Department of Medicine, University of California, San Diego, La Jolla, CA 92093, USA.

[6] Department of Pathology, Beth Israel Deaconess Medical Center, Harvard Medical School, Boston, MA 02215, USA.

[7] Center for Interdisciplinary Cardiovascular Sciences, Cardiovascular Division, Department of Medicine, Brigham and Women's Hospital, Harvard Medical School, Boston, MA 02115, USA.

* Correspondence: Hong Chen, Ph.D., Vascular Biology Program, 1 Blackfan Circle, Karp 12214, Mailstop: 3137, Boston, MA   02115. Tel.: (617) 919-6304. E-mail: hong.chen@childrens.harvard.edu

\# Present Address: Department of Medicine and Hastings Center for Pulmonary Research, Keck School of Medicine, University of Southern California, Los Angeles, CA 90033, USA

Short Title: Endothelial FoxM1 and Dab2 induces Diabetic Wound Healing

1 Abstract

2 Diabetes mellitus can cause impaired and delayed wound healing, leading to lower extremity
3 amputations; however, the mechanisms underlying the regulation of vascular endothelial growth
4 factor (VEGF)-dependent angiogenesis remain uncertain and could reveal new therapeutic
5 targets. In our study, the molecular underpinnings of endothelial dysfunction in diabetes were
6 investigated, focusing on the roles of Disabled-2 (Dab2) and Forkhead Box M1 (FoxM1) in
7 VEGF receptor 2 (VEGFR2) signaling and endothelial cell (EC) function. Bulk RNA-sequencing
8 analysis identified significant downregulation of Dab2 in high concentrations glucose treated
9 primary mouse skin ECs, simulating hyperglycemic conditions in diabetes mellitus. In diabetic
10 mice with a genetic EC deficiency of Dab2 angiogenesis was reduced *in vivo* and *in vitro* when
11 compared with wild-type mice. Restoration of Dab2 expression by injected mRNA-containing
12 lipid nanoparticles rescued impaired angiogenesis and wound healing in diabetic mice. At the
13 same time, FoxM1 was downregulated in skin ECs subjected to high glucose conditions as
14 determined by RNA-sequencing analysis. FoxM1 was found to bind to the Dab2 promoter,
15 regulating its expression and influencing VEGFR2 signaling. The FoxM1 inhibitor FDI-6
16 reduced Dab2 expression and phosphorylation of VEGFR2. These findings indicate that
17 restoring Dab2 expression through targeted therapies can enhance angiogenesis and wound repair
18 in diabetes. To explore this therapeutic potential, we tested LyP-1-conjugated lipid nanoparticles
19 (LNPs) containing Dab2 or control mRNAs to target ECs and found the former significantly
20 improved wound healing and angiogenesis in diabetic mice. This study provides evidence of the
21 crucial roles of Dab2 and FoxM1 in diabetic endothelial dysfunction and establishes targeted
22 delivery as a promising treatment for diabetic vascular complications.

23

24 Introduction

25 One of the most serious pathological outcomes of diabetes mellitus is impaired and/or delayed
26 wound healing, which – in severe cases – can lead to lower extremity amputations (LEAs)[1-3].
27 Although the etiological basis of chronic non-healing wounds is multi-faceted, aberrant
28 angiogenesis is, at least in part, involved in sustaining this phenotype. During wound healing,
29 angiogenic sprouts descend upon the wound area to establish normoxia and they eventually
30 fashion a microvascular network to restore oxygen and nutrient delivery to the wound area and
31 help remove debris[4-6]. Therefore, promoting angiogenesis is crucial for wound healing, and
32 developing effective targets for angiogenesis could benefit millions of diabetic patients.

33 Vascular endothelial growth factor (VEGF) is a critical angiogenic factor that signals through
34 VEGF receptors (VEGFRs)[7]. Among the family of VEGFRs, VEGFR2 potentiates angiogenesis
35 more potently than other VEGFRs. Binding of VEGF to VEGFR2 leads to the phosphorylation
36 of VEGFR2 and activation of downstream signaling pathways, including MAPK/ERK and
37 PI3K/Akt, which promote endothelial cell (ECs) proliferation, migration, and survival[8,9]. In
38 diabetic conditions, there is a decrease in VEGF-induced phosphorylation of VEGFR2 and
39 downstream signaling, leading to impaired angiogenesis[10-12]. Hence, gaining insights into the

40 regulation of VEGFR2-dependent angiogenesis may lead to the identification of new therapeutic
41 strategies in this context.

42 Several studies have shown that the highly-conserved adaptor protein Disabled Homolog 2
43 (Dab2) plays a direct role in regulating VEGF signaling in ECs[13,14]. Dab2 is involved in the
44 regulation of endocytosis and lysosomal degradation of receptor tyrosine kinases, including
45 VEGFR2. Dab2 binds to the cytoplasmic tail of VEGFR2 and promotes its endocytosis and
46 recycling[14]; thereby, serving to enhance VEGFR2-mediated angiogenesis. In spite of this, the
47 specific structural domain through which Dab2 interacts with VEGFR2 is unknown. At the same
48 time, the molecular mechanisms underlying Dab2-mediated angiogenesis, particularly in the
49 context of wound healing in diabetes, is not clear. Identifying factors that regulate Dab2
50 transcription is key to uncovering the mechanisms of Dab2's role in endothelial cell angiogenesis
51 under diabetic conditions. More pressingly, it remains unknown if modifying Dab2 levels could
52 serve as a therapeutic strategy to enhance diabetic wound healing. To better target Dab2, it is
53 essential to develop exogenous supplementation methods that have a shorter half-life and higher
54 efficiency.

55 The present study was designed to dissect the potential involvement of Dab2 in regulating VEGF
56 signaling during angiogenesis in the context of wound healing in diabetes. Using an EC-specific
57 Dab2 knockout mouse model, we found that the Forkhead box M (FoxM1) regulates Dab2
58 expression in ECs and promotes diabetic wound healing. This transcription factor orchestrates
59 the expression of genes essential for cell cycle progression, thus facilitating cell growth and
60 division; a process that is vital for tissue repair and regeneration[15-18]. We found that FoxM1
61 positively regulates Dab2 expression by directly binding to its promoter to influence
62 transcription and protein levels of Dab2. By injecting Dab2-mRNA encapsulated in lipid
63 nanoparticles (LNPs), or using the FoxM1 inhibitor FDI-6, wound healing was significantly
64 enhanced through increased angiogenesis, which could lay the foundation for the development of
65 novel therapies to enhance angiogenesis in diabetes.

66 Together, our results suggest that Dab2 plays a critical role in VEGF signaling and angiogenesis
67 in ECs under diabetic conditions by regulating the activation of VEGFR2. We also identified the
68 specific binding domain of Dab2 that binds to VEGFR2 and demonstrated that FoxM1 regulated
69 transcription of this adaptor protein in ECs. Our findings indicate that Dab2 may represent a
70 previously unidentified potential target for improving diabetic wound healing.

71

72 **Methods**

73 **Mouse models**

74 All animal experiments were approved by the Institutional Animal Care and Use Committee at
75 Boston Children's Hospital. To produce EC-specific Dab2KO (Dab2-EC^{iKO}) mice, a breeding
76 strategy was employed using Dab2$^{fl/fl}$ mice and EC-specific Cre transgenic CDH5-Cre mice. To
77 activate Cre recombinase, 8 to 10 week old mice received 4-hydroxytamoxifen (Hello Bio,

78 dissolved in a 9:1 mixture of DMSO and ethanol at a dosage of 5–10 mg/kg body weight) seven
79 times every other day. For induction of diabetes, mice underwent intraperitoneal injection with a
80 low-dose of streptozotocin (STZ, Sigma-Aldrich, 50 mg/kg) following an established protocol[19].
81 Hyperglycemia was confirmed when mice maintained a fasting blood glucose level above 200
82 mg/dL for over a week post-STZ administration. After inducing diabetes, the mice were placed
83 on a high-fat diet (HFD, 60 kcal% fat from Research Diets Inc.).

Cell cultures

85 Primary mouse ECs were obtained from mouse skin and cultured according to previously
86 established protocols with some modifications[19-21]. Briefly, to isolate ECs from the skin, 4-6
87 mice aged 2-3 months were used. The mice were anesthetized with isoflurane and humanely
88 euthanized by cervical dislocation. The skin was excised from the mice using surgical scissors or
89 a scalpel, then diced into small fragments on ice and subjected to enzymatic digestion with
90 collagenase Type IV (2 mg/mL; Gibco Laboratories) in a 37°C water bath with agitation (10
91 rpm) for a duration of 60-90 minutes. Digestion was stopped by adding an equal volume of ice-
92 cold FBS. The resulting digested tissue was filtered through a 40 µm cell strainer (BD) to
93 separate the cells from debris. The resulting cell suspension was then centrifuged at 400 g for 5
94 minutes at 4°C. 10 µL anti-mouse CD31 MicroBeads (Miltenyi Biotec) were added into about
95 10^7 isolated cells in 90 µL of buffer (PBS, pH 7.2, 0.5% BSA, and 2 mM EDTA). The cell
96 mixture was then incubated for 15 minutes at 4 °C. These isolated cells were utilized for
97 downstream experiments. The primary ECs used in all experiments were isolated and maintained
98 between 1-6 passages. Cells were treated with normal glucose (5 mmol/L) or high glucose (20
99 mmol/L) medium for ~48 hours. ECs derived from wild-type mice or mice carrying Dab2$^{fl/fl}$;
100 iCDH5-ER^{T2} Cre alleles were exposed to 5 µmol/L of 4-hydroxytamoxifen (dissolved in ethanol)
101 for two days at 37°C. Following treatment, cells were incubated for another two days without 4-
102 hydroxytamoxifen. Confirmation of Dab2 deletion was carried out by Western Blotting.

Mouse corneal micropocket angiogenesis assay

104 The corneal micropocket angiogenesis assay in mice was carried out following established
105 protocols[19,22]. Briefly, mice were anesthetized using Avertin (400-500 mg/kg delivered by
106 intraperitoneal injection i.p.). An incision into the cornea was gently created at an approximately
107 30° angle and 0.7 - 1.0 mm from the limbus using a corneal blade and a stereoscope. A sustained-
108 release pellet containing the volume of 0.4 mm x 0.4 mm x 0.2 mm pellet of VEGFA (~ 20 ng,
109 BioLegend) was implanted into the pocket. 5 -7 days post-implantation, the corneas were
110 excised, and stained with PE-conjugated anti-CD31 antibody (1:100, BD Pharmingen) to
111 highlight limbal blood vessels. The growth of these vessels was quantified by measuring the
112 growth pixels using the Vessel Analysis plugin in ImageJ.

RNA isolation

114 Total RNA was isolated from the cells using a commercially-available kit (Qiagen, Valencia, CA,
115 USA) according to the manufacturer's instructions. RNA quantity and quality was determined
116 using a NanoDrop 2000 spectrophotometer (Thermo Fisher Scientific, Waltham, MA, USA).

Library preparation and bulk RNA sequencing

Total RNA was extracted from the collected samples and assessed for quality and integrity. Quality control of all RNA-seq samples was performed at the Harvard Medical School Biopolymer Facility using a 2100 Bioanalyzer (Agilent). Samples with an RIN score greater than 7 were considered for further processing. The NEBNext Poly(A) mRNA Magnetic Isolation Module was used to enrich poly(A)+ mRNA from the total RNA pool, using Oligo d(T)25 beads for magnetic separation. Post isolation, the mRNA was eluted and either used immediately or stored at -80°C for subsequent experiments. Library preparation began with reverse transcription of the enriched mRNA into cDNA, followed by end-repair and the addition of a single 'A' nucleotide at the 3' ends. NEBNext Adaptors were then ligated to the cDNA, and unique indices were added using the NEBNext Multiplex Oligos for Illumina to allow for sample multiplexing during sequencing. The adaptor-ligated cDNA was used for PCR amplification, and the product was purified to remove any remaining enzymes and primers. The final library was validated for quality using capillary electrophoresis and quantified through qPCR. Libraries were pooled in equimolar ratios, as determined by the quantification results, before being forwarded to the sequencing facility for high-throughput analysis. The RNA library was sequenced using the HiSEQ Next-generation Sequencing System with a read length of 75 at the core facility of Azenta Life Sciences.

Bulk RNA-seq data analysis

Sequencing data were processed using Trimmomatic software. Low-quality reads were removed to retain only high-quality sequences for analysis. These clean reads were then aligned to the mouse reference genome GRCm38 (mm10) using the HISAT2 alignment tool. StringTie was used to enumerate the reads for each gene. The edgeR package in R was used to identify genes with significant changes in expression, with significant differences being noted at an adjusted p-value of less than 0.05. Pathway and gene function analyses were performed using Gene Set Enrichment Analysis (GSEA), with significance attributed to terms with an adjusted p-value and FDR below 0.05. Genes were categorized in the volcano plot based on the degree of expression change and statistical significance, with colors assigned accordingly.

qRT-PCR

Total RNA was isolated from primary mouse ECs using a commercially available kit (Qiagen, Valencia, CA, USA) followed by DNase I treatment. The RNA was then reverse transcribed into cDNA using Oligo (dT) 20 Primers (Invitrogen) as per the manufacturer's protocol. Quantitative real-time PCR was performed using the StepOnePlus Real-Time PCR detection system (Applied Biosystems, Foster City, CA, USA) and SYBR Green qPCR super Mix (Invitrogen). The PCR amplification cycles consisted of an initial heating step at 95°C for 10 min, followed by 40 cycles of 15 s at 95°C, 1 minute at 60°C, and 45 s at 72°C. The relative abundance of mRNA was determined using the average threshold cycles (Ct) of samples normalized to β-actin mRNA. Each sample was analyzed in triplicate. The mouse primer sequences used for PCR are shown in Table S1.

RNA Interference

The study used RNA interference (RNAi) to knockdown the expression of specific genes in primary ECs. ON-TARGETplus Mouse Dab2 siRNA (Horizon, J-050859-09-0002) and its respective ON-TARGETplus non-targeting siRNAs (Horizon, D-001810-0X) were transfected in the isolated ECs using either Oligofectamine or RNAiMAX according to the manufacturer's instructions (Invitrogen). The cells were processed for biochemical immunoprecipitations or immunofluorescence assays 48-72 hours after transfections as previously described [23].

Glucose tolerance test (GTT)

Glucose tolerance was tested as described previously[19]. Mice were fasted for 16 hours. The weight of each mouse determined the calculated glucose dose at a ratio of 2 g/kg body weight. Injection volume into the peritoneal of mouse = BW(g)×10μL of 250mg/mL glucose solution. Tail snipping was used to collect blood samples. Blood glucose was determined by glucometer in tail vein blood. Blood glucose is measured at 0, 30, 60, 90, and 120 minutes after glucose injection.

Insulin tolerance test (ITT)

Insulin tolerance was tested as described previously[19]. Mice are fasted for 3 hours. The weight of each mouse determined the calculated insulin dose at a ratio of 0.75 U/kg body weight. Insulin was prepared at 0.1 U/mL in advance (16.6μL of 10 mg/mL insulin in 40 mL PBS). Injection volume into the peritoneal of mouse = BW(g) X 7.5μL of 0.1U/mL insulin solution. Tail snipping is used to obtain blood and glucose levels were determined using a glucometer. Measurements were made at 0, 15, 30, 60, 90, and 120 minutes after insulin injection.

LyP-1 peptide-linked Dab2 and control mRNA lipid nanoparticles

LyP-1 peptide was conjugated to DSPE-PEG via an NHS-amine reaction[24-27]. Briefly, the activated DSPE-PEG-NHS was mixed with Lyp1 in 1x PBS buffer solution (pH 7.4) at room temperature and stirred for 24 hours. These crude products were dialyzed against water for 3 days (MWCO, 3 kDa), followed by lyophilization. Successful conjugation was confirmed using proton nuclear magnetic resonance (1H NMR)[28].

Lipid nanoparticles (LNPs) containing mRNA, including LNPs-Lyp1-Dab2 mRNA and LNPs-Lyp1-GFP mRNA were formulated by mixing an aqueous phase containing mRNA and an organic ethanol phase containing MC3, 1,2-dioleoyl-sn-glycero-3-phosphoethanolamine (DOPE), cholesterol, and PEG-conjugated lipids (DMG-PEG and DSPE-PEG) [29,30]. Briefly, one volume of lipid mixtures (MC3, DOPE, Chol, DMG-PEG, and DSPE-PEG-LyP1 at a molar ratio of 50:10:38: 1:1) in ethanol and three volumes of mRNA (Dab2 mRNA or GFP mRNA, 1:10 w/w mRNA to lipid) containing sodium acetate buffer (50 mM, pH 4) were mixed thoroughly and stirred at RT for 20 min. The resulting LNPs-Lyp1-Dab2 mRNA and LNPs-Lyp1-GFP mRNA were further purified by ultrafiltration (MWCO, 10 kDa) with 1x PBS (pH7.4) to remove naked mRNAs and ethanol. The final mRNA-loaded LNPs were maintained in 1x PBS at an mRNA concentration of 75 μg/mL[30]. Dynamic light scattering (DLS) was adopted to

194 characterize the LNPs-Lyp1-Dab2 mRNA and LNPs-Lyp1-GFP mRNA[29,31]. As shown in Fig.
195 S3B, the average sizes were 136.7 ± 2.52 nm for LNPs-Lyp1-Dab2 mRNA and 120.5 ± 2.45 nm
196 for LNPs-Lyp1-GFP mRNA, with zeta potentials of -5.54 ± 0.17 mV and -6.11 ± 0.51 mV,
197 respectively.

Injection of LNPs into mice

199 Dab2 mRNA was loaded into LNPs to facilitate the *in vivo* application by protecting mRNA
200 from enzymatic degradation, enhancing cellular uptake and endosomal escape, and/or improving
201 systemic circulation. This encapsulation process was crucial to maintain the stability and
202 effectiveness of the Dab2 mRNA for its use in living organisms. The prepared Dab2-mRNA
203 LNPs (LNPs-Lyp1-Dab2 mRNA or control LNPs-Lyp1-GFP mRNA) were administered to mice
204 by intravenous (i.v.) injection, with a dosage of 15 μg per mouse. These treatments were given
205 twice a week for a total of four weeks.

Lentivirus-mediated Dab2 overexpression

207 Lentivirus for Dab2 overexpression was produced using the PEI STAR transfection method [32-35]
208 in ECs. Initially, ECs were seeded in a 10 cm dish and incubated at 37°C with 5% CO_2 until they
209 reached 60-70% confluence. For transfection, a mixture containing equimolar amounts of
210 pMD2.G (VSVg) and pSPAX2 (Gag and Pol) and, along with a double molar amount of
211 pGenLenti Dab2-Flag transfer vector was prepared for a total of 10 μg of DNA. This DNA
212 mixture was combined with 30 μL of PEI STAR (1 mg/mL) in 500 μL of fresh medium, and
213 incubated for 10 minutes, and then added dropwise to the cells. After 24 hours, the medium was
214 replaced to remove residual transfection reagent, and the process was repeated after 48 hours.
215 After 72 hours of transfection, the supernatant containing the viral particles was harvested and
216 centrifuged to remove cell debris, which was filtered through a 0.45 μm filter and stored at -80°C
217 for subsequent experiments.

CRISPR/Cas9-mediated mutations to block FoxM1 binding to the mouse *Dab2* promoter

219 CRISPR/Cas9-mediated gene editing was employed to introduce targeted mutations within the
220 Dab2 promoter region of mouse skin ECs to disrupt the FoxM1 binding site. The
221 Ad5CMVspCas9/RSVeGFP vector was purchased from the Viral Core at the University of Iowa,
222 using the expression of SpCas9 and a GFP reporter. The selected sgRNA sequences: sgRNA1:
223 TAAGATTCTCTACTATGTG (+ Strand); sgRNA2: TTGTATATATCTTGGGGAA (- Strand). A
224 1,154 bp DNA fragment with three FoxM1 transcription factor binding sites spans from -4,806
225 bp to -5,906 bp upstream of the transcription start site (TSS) of Dab 2. The synthetic DNA
226 fragment containing mutations in the PAMs and FoxM1 binding sites was obtained from
227 Synthego. To prevent FoxM1 from binding to the Dab2 promoter and verify whether cell
228 transduction is successful, the three binding sites of FoxM1 were mutated into restriction enzyme
229 sites in the synthetic DNA fragment, as follows: Site 1: Sal1 restriction site (AAATGC ->
230 GTCGAC); site 2: Fsp1 restriction site (CAATGC -> TGCGCA); site 3: Sal1 restriction site
231 (TAATGA -> GTCGAC).

For the transduction of ECs, the Ad5CMVspCas9/RSVeGFP vector was introduced using Lipofectamine 3000 (Thermo Fisher Scientific) to maintain the integrity and viability of cells. After 3 days, the synthetic DNA recombination fragment DNA fragment was introduced into the ECs employing the Amaxa Nucleofector 1 Electroporation System and associated kit, strictly adhering to the manufacturer's protocol. The electroporation conditions were optimized to ensure high viability and efficient uptake of the DNA constructs. After transfection, cells were cultured under standard conditions and screened for GFP expression using fluorescence microscopy. DNA isolated from transduced EC cells was then digested with restriction enzymes to further confirm successful delivery and expression of CRISPR components.

ChIP-PCR

Following genomic editing, ChIP-PCR was performed to verify the impact of mutation on FoxM1 binding to the Dab2 promoter. The ChIP procedure made use of a kit (Abcam), starting with cell fixation, chromatin shearing by sonication, and immunoprecipitation with specific antibodies targeting FoxM1. The DNA-protein complexes were pulled down using protein A beads, and the DNA was purified and analyzed by PCR to assess the binding activity of FoxM1 at the modified Dab2 promoter. The ChIP-PCR primers of Dab2 are as follows: Forward: 5'-CCCAGCAGTACAAGTCTGGA-3'; Reverse: 5'-AGGACTGAGTGGACATGGTG-3'.

Western blot analysis

To extract total proteins, cells were lysed using RIPA buffer. Equal amounts of denatured protein were loaded onto a 10% SDS-PAGE gel for electrophoresis. The separated proteins were then transferred to a PVDF membrane and blocked with 5% skimmed milk for 30 minutes at room temperature. Primary antibodies were diluted at 1:1000 and the secondary antibodies were diluted at 1:2000. The antibodies are listed in Table S2.

Immunofluorescence staining

For immunofluorescence staining, primary mouse ECs were cultured on glass coverslips and fixed in 4% paraformaldehyde (PFA) for 10 minutes. The cells were then permeabilized with 0.3% Triton X-100 in phosphate-buffered saline (PBS) for 10 minutes and blocked in a solution containing 5% donkey serum in PBS for 1 hour at room temperature. The primary antibodies were diluted in blocking solution and incubated with the cells overnight at 4°C. The next day, the coverslips were washed with PBS and incubated with the respective secondary antibodies conjugated to fluorescent labels (Alexa Fluor) for 2 hours at room temperature. After washing with PBS, the coverslips were mounted on glass slides using Vectashield mounting medium with DAPI and visualized using a fluorescence microscope (Zeiss LSM 880) with appropriate filters. Images were acquired using a digital camera (Zeiss AxioCam). Unless otherwise specified, secondary antibodies for immunohistochemistry were applied at a concentration of 1:200. The antibodies are listed in Table S2.

***In vitro* wound healing assays**

An *in vitro* scratch wound healing assay was performed to evaluate the migration of wild type

270   and Dab2-EC^{iKO} cells under normoglycemic and hyperglycemic conditions. Cells were seeded in
271   a 24-well plate and grown to confluence. A scratch wound was made in the cell monolayer using
272   a sterile pipette tip, and the cells were washed to remove any detached cells. The cells were then
273   cultured in either a normoglycemic media (5 mmol/L glucose) or a hyperglycemic media (20
274   mmol/L glucose) in the presence or absence of VEGFA (100ng/mL) and images were taken at
275   specified time points to monitor cell migration into the wound area. The rate of cell migration
276   was calculated by measuring the width of the wound at different time points. The differences in
277   wound closure between wild type and Dab2-EC^{iKO} cells under both normoglycemic and
278   hyperglycemic conditions were analyzed.

Vascular network formation assays

280   An *in vitro* Matrigel assay was performed to compare the behavior of wild type and Dab2-EC^{iKO}
281   cells in normoglycemic and hyperglycemic conditions. The cells were seeded on top of a
282   Matrigel matrix in a 24-well plate and cultured in a normoglycemic media (5 mmol/L glucose) or
283   a hyperglycemic media (20 mmol/L glucose) for a specified period. The cells were fixed and
284   analyzed to determine morphological changes and quantify cell migration and proliferation. The
285   differences in behavior between the wild type and Dab2-EC^{iKO} cells were analyzed under both
286   normoglycemic and hyperglycemic conditions.

EdU staining

288   An EdU staining assay was performed to determine the cell proliferation of wild type and Dab2-
289   EC^{iKO} cells under normoglycemic and hyperglycemic conditions. The cells were cultured in
290   either a normoglycemic media (5 mmol/L glucose) or a hyperglycemic media (20 mmol/L
291   glucose) and then incubated with EdU, a thymidine analog, for 4 hours in presence or absence of
292   VEGFA (100 ng/mL). The cells were then fixed and processed for staining, including the
293   addition of a DAPI stain to visualize the nuclei. The EdU-incorporated cells were identified by
294   fluorescence using a specific antibody. The number of EdU positive cells was counted and
295   compared between the wild type and Dab2-EC^{iKO} cells under both normoglycemic and
296   hyperglycemic conditions. The differences in cell proliferation were analyzed and quantified.

***In vivo* wound healing assays**

298   A dermal wound healing assay was performed to evaluate the role of the Dab2 gene in the wound
299   healing process. Two groups of mice, wild type and Dab2-EC^{iKO}, were used in this study. A
300   standardized wound was created on the dorsal surface of each mouse using a surgical blade. The
301   mice were then monitored for approximately 7 days to evaluate wound healing, including
302   changes in wound size and tissue regeneration. At the end of the study, the mice were sacrificed,
303   and the wound sites were collected for further analysis. The collected tissue was processed for
304   histological analysis, including the use of specific stains to evaluate vascular density during
305   wound closure. The differences in wound healing response between the wild type, diabetic, and
306   Dab2-EC^{iKO} mice were analyzed and quantified.

Matrigel plug assays

308 An *in vivo* Matrigel assay was performed to study the angiogenic response of wild type and

309 Dab2-EC[iKO] mice. Matrigel mixed with 100 ng/mL VEGFA was prepared, and 400 - 500 µL was

310 implanted subcutaneously into the back of both wild type and Dab2-EC[iKO] mice. The mice were

311 then monitored for 7 days to evaluate angiogenic response, including the formation of blood

312 vessels in the implantation site. At the end of the study, the mice were sacrificed, and the

313 implantation sites were collected for further analysis. The collected tissue was processed for

314 histological analysis, including the use of specific stains to visualize blood vessels and quantify

315 angiogenic response. The differences in angiogenic response between the wild type and Dab2-

316 EC[iKO] mice were analyzed and quantified. This assay provided valuable information on the role

317 of the Dab2 gene in modulating angiogenic response *in vivo*.

318 **Dab2 inhibitors predicted by molecular modeling**

319 To predict the Dab2 signaling inhibitors, docking experiments were performed using the ClusPro

320 2.0 program[36,37]. The 3-D structure of Dab2 PTB domain (PDB ID: 2LSW) was docked into

321 VEGFR2 Kinase domain (PDB ID: 3U6J) to generate the predicted binding models of

322 Dab2:VEGFR2 (Table 1). Models with the highest scores and best topologies were selected for

323 the proposed models of the interaction between Dab 2 and VEGFR2. In the interaction models, a

324 total of 6 Dab2 inhibitory peptides were identified with good scores based on the molecular

325 modeling (Fig. 3H-I).

326 **Statistics**

327 Results were presented as the mean ± SD. The evaluation of differences between groups was

328 performed using Student's t-test with the demonstration of homogeneity of variance. The one-

329 way ANOVA was used for multiple comparisons followed by Dunnett's post hoc analysis, by

330 GraphPad Prism 8. A p-value of less than 0.05 was considered for statistical significance.

331

332 **Results**

333 **Diabetes and high glucose treatment in ECs leads to the downregulation of Dab2**

334 Given the crucial roles in both physiological and pathological angiogenesis, we sought to

335 determine if endocytic adaptor proteins were also involved in mitigating aspects of diabetic

336 angiogenesis. To address this goal, we isolated CD31-enriched primary mouse endothelial cells

337 (ECs) and treated them with normal (5 mmol/L) or high glucose concentrations (20 mmol/L), a

338 condition mimicking hyperglycemia in diabetes mellitus, for a period of 48 hours, followed by

339 bulk RNA-sequencing analysis. Differential gene expression analysis revealed 168 significantly

340 downregulated and 386 significantly up-regulated genes in the ECs grown in high glucose

341 culture conditions compared to ECs cultured in normal glucose media (Fig. 1A, S1A). Volcano

342 plot analysis revealed downregulation of the Dab2 mRNA levels in high glucose-treated ECs

343 compared to the control group (Fig. 1A). Further corroborating these findings, quantitative PCR

344 (qPCR) analysis showed that high glucose treatment or ECs from diabetic mice resulted in the

345 downregulation of Dab2 (Fig. 1B-C).

346 GSEA identified multiple downregulated genes in the high-glucose treatment group that are
347 involved in the regulation of cell cycle progression such as E2F target, G2-M checkpoint, and
348 mitotic spindle formation genes. Additionally, genes involved in cell growth, such as components
349 of mTORC1 (mechanistic target of rapamycin complex 1) signaling and Myc target genes were
350 downregulated (Fig. S1B-S1D). Consistent with the downregulation of Myc target genes, a
351 majority of metabolic genes and genes involved in metabolic processes, including glycolysis and
352 oxidative phosphorylation, were downregulated in ECs treated with a high concentration of
353 glucose (Fig. S1B). This suggests that aerobic glycolysis, a process usually coupled with cell
354 proliferation and growth, is impaired in the presence of a high concentration of glucose.
355 Consistent with the RNA results, western blot analysis revealed significantly downregulated
356 Dab2 protein levels in the diabetic group or high glucose treated group compared to non-diabetic
357 controls (Fig. 1D-G). Downregulation of Dab2 expression in diabetic conditions was also
358 confirmed by immunostaining of skin ECs cultured in normal or high glucose concentrations
359 (Fig. 1H-I). Together, these *in vitro* observations suggest that hyperglycemic ECs exhibit
360 downregulation of Dab2 mRNA and protein levels, along with reduced expression of genes
361 involved in cellular metabolism, growth, and proliferation.

362 **EC-specific Dab2 knockout cause reduced angiogenesis *in vivo***

363 To test Dab2 function in diabetic mice we utilized a Matrigel transplantation technique where
364 VEGFA-infused Matrigel was implanted into both wild-type (WT) and diabetic mice to create a
365 conducive setting for *in vivo* angiogenesis analysis. This approach revealed that in the diabetic
366 mice, the angiogenic blood vessels within the VEGFA-infused Matrigel exhibited a notable
367 decrease in Dab2 levels compared to those in the WT mice, indicating the impact of diabetes on
368 Dab2 expression and its potential role in angiogenesis (Fig. 2A-C). To determine if the pro-
369 angiogenic effects of Dab2 were associated with enhanced wound healing responses *in vivo*, we
370 examined the effects of EC-specific Dab2 deficiency on wound healing under physiological and
371 diabetic conditions (Fig. 2C). Mice were treated with STZ and fed a high-fat diet to prepare the
372 diabetic mouse model. Diabetes is induced by an intraperitoneal injection of STZ, with low-dose
373 insulin given subcutaneously to manage mortality[38]. STZ selectively damages insulin-producing
374 beta cells in the pancreas, leading to reduced insulin secretion and hyperglycemia. When used
375 alongside an HFD, which induces insulin resistance by causing obesity, this method effectively
376 simulates the metabolic conditions of Type 2 diabetes, eliciting both insulin resistance and
377 compromised insulin production; thereby, creating a comprehensive diabetic mouse model.

378 Glucose and insulin tolerance tests (ITTs and GTTs) were performed in WT mice and Dab2-
379 EC^{iKO} mice with or without STZ injection and HFD feeding. It was found that EC-specific Dab2
380 deficiency led to more severe insulin resistance and higher blood glucose than WT mice (Fig
381 S2A-B). Wounds were inflicted in the dorsal skin of normal or diabetic WT or Dab2-EC^{iKO} mice
382 with a disposable biopsy punch under sterile conditions. Each wound was photographed at the
383 indicated times and analyzed. EC-specific Dab2-deficiency was consistently associated with
384 delayed wound healing response compared to WT mice (Fig. 2D-F). Whereas diabetic conditions
385 hampered wound healing in WT mice, Dab2-EC^{iKO} diabetic mice displayed the slowest wound

386 healing rate among all the groups. Consistently, CD31-specific immunofluorescence staining of
387 wounds isolated on day 7 post-wound creation revealed significantly less vascularization of the
388 wound area in diabetic and Dab2-EC^{iKO} mice (Fig. S2C-D).

389 To evaluate the effect of Dab2 on neovascularization *in vivo*, we subcutaneously implanted
390 Matrigel plugs containing VEGFA into Dab2-EC^{iKO} and WT adult diabetic or control mice to
391 directly examine EC migration and network formation *in vivo*. Consistently, the diabetic and
392 Dab2-EC^{iKO} groups showed significantly reduced vascularization compared to WT controls (Fig.
393 2G-H). Furthermore, Matrigel from diabetic WT mice exhibited reduced vascularization to a
394 similar extent to that in Dab2-EC^{iKO} mice.

395 To further investigate the impact of EC-specific Dab2-deficiency on angiogenesis, we performed
396 a neo-angiogenesis assay induced by exogenous supplementation of VEGFA in the cornea using
397 a corneal micro-pocket assay. Immunofluorescence staining of whole-mount corneas with a
398 CD31-specific antibody confirmed the impaired vascularization and revealed reduced vessel
399 density in Dab2-EC^{iKO} and diabetic mice (Fig. 2I-J). Specifically, we observed a significant
400 decrease in the number of EdU-positive cells in the cornea of diabetic and Dab2-EC^{iKO} mice,
401 indicative of a reduction in the proliferative response of ECs to VEGFA stimulation (Fig. 2K).
402 Taken together, these observations demonstrate that EC Dab2 plays a significant role in
403 promoting VEGFA-driven angiogenesis and wound healing *in vivo*.

404 **Dab2 downregulation in ECs cause reduced angiogenesis *in vitro***

405 To further investigate the role of Dab2 in angiogenesis, we isolated skin ECs from WT and
406 Dab2-EC^{iKO} mice and treated them with tamoxifen. We performed *in vitro* proliferation (EdU
407 labeling), scratch-wound healing, and EC tube formation in Matrigel in normal or high glucose
408 media in the presence of VEGFA. The EdU-positive cells were significantly decreased in Dab2-
409 deficient ECs compared to WT controls. Moreover, high glucose treatment led to a reduced
410 number of EdU-positive cells in WT ECs compared to that cultured in the media with normal
411 glucose concentration (Fig. 3A-B). Likewise, the *in vitro* scratch wound healing assay
412 demonstrated that Dab2-deficient ECs exhibited a slower rate of wound closure compared to WT
413 ECs. High-concentration glucose treatment of WT ECs led to blunted scratch wound closure like
414 ECs from Dab2-EC^{iKO} mice (Fig. 3C-D). Similarly, the *in vitro* tube formation assay revealed
415 that Dab2-deficient ECs formed fewer and less organized networks in the presence of VEGFA
416 compared to WT ECs. (Fig. 3E-F). These findings suggest that Dab2 plays a crucial role in
417 regulating the proliferation and migration of skin ECs under both normal and diabetic conditions.
418 Inhibition of Dab2 expression likely underlies the compromised angiogenic function in ECs
419 exposed to hyperglycemia in diabetes mellitus.

420 Dab2 is known to affect various cellular processes and is a critical regulator of VEGFR2
421 signaling. A previous study has shown that Dab2 could affect the VEGFR2 signaling pathway in
422 glomerular endothelial cells[13]. However, the binding domain of Dab2 with VEGFR2 is not clear.
423 To determine whether Dab2 could activate VEGFR2 signaling in angiogenesis and determine the
424 precise binding domain involved in this activation, we next sought to determine exogenous

425 inhibition of Dab2 with an inhibitory peptide (DPI) that could impede VEGFR2 signaling. We
426 predicted a minimal peptide stretch in the Dab2 PTB domain, which is predicted to associate
427 with VEGFR2, would abolish the interaction between VEGFR2 and Dab2 under various
428 conditions. Using structural bioinformatics and molecular modeling, the study analyzed the
429 alignment of human, rat, and mouse Dab1 and Dab2, identifying a consistent RGD motif and an
430 additional KGD motif in the Dab2 PTB domain, suggesting integrin binding capabilities (Fig.
431 3G-H). Wild type mouse endothelial cells were pre-treated with DPI or control peptides for 18 h,
432 followed by VEGFA stimulation. Consistent with the observations made in Dab2-depleted ECs,
433 the DPI peptide significantly reduced the levels of pVEGFR2, pAkt, and pERK relative to the
434 control peptide (Fig. 3I). Together, these results suggest that Dab2 plays a crucial role in
435 regulating the VEGF-VEGFR2 signaling pathway in EC angiogenesis.

Restoration of Dab2 Expression in ECs Rescues Impaired Angiogenesis and Wound
Healing in Diabetic Mice

438 To investigate the therapeutic efficacy of Dab2 restoration in diabetic conditions, we conducted a
439 rescue experiment in STZ-induced diabetic mice. We intravenously administered Dab2-mRNA
440 encapsulated in LNPs conjugated with Lyp1 peptide at a dose of 15 μg/mouse, twice a week,
441 during the wound healing period (Fig. S3). This treatment was aimed at restoring Dab2
442 expression and enhancing angiogenesis and wound healing. Diabetic mice treated with LNPs-
443 LyP1-Dab2-mRNA exhibited significantly accelerated wound healing activity compared with the
444 untreated diabetic mice (Fig. 4A-B). The treated group exhibited accelerated wound closure and
445 healing rates, with most wounds nearly fully healed by day 7, in contrast to the control group
446 (LNPs-LyP1-GFP mRNA), where wound healing was significantly impeded within the same
447 time. To complement these *in vivo* findings, we utilized a Dab2-Lentivirus system to overexpress
448 Dab2 in high glucose-treated primary skin ECs enriched from adult mice. Dab2 overexpression
449 in high glucose treatment recovered the proliferative capacity in ECs compared to control (Fig.
450 4C-D). We also performed scratch assays and tube formation assays to mimic wound healing and
451 angiogenesis *in vitro* (Fig. 4E-H). Cells overexpressing Dab2 tended to form more organized and
452 complex tube-like structures, as revealed by tube formation assays (Fig. 4E-F) and exhibited
453 increased migratory behavior in scratch assays (Fig. 4G-H), compared to control cells. These
454 results confirmed the ECs autonomous pro-angiogenic function of Dab2 and highlight the
455 potential therapeutic utility of overexpressing Dab2 to restore impaired angiogenic responses in
456 diabetic conditions.

FoxM1 is downregulated in diabetes and regulates Dab2 transcription

458 To find the mechanism of Dab2 regulation, we further explored the RNA sequencing data in
459 Figure 1. Volcano plot analysis revealed downregulation of transcription factors involved in cell
460 proliferation and growth, including FoxM1 (Forkhead box M1), Egr2 (Early growth response
461 protein 2), Hes1 (Hairy and enhancer of split 1), Etv4 (ETS variant 4 exclusively in the high
462 glucose-treated samples compared with the control group (Fig. 5A, S1A). qPCR analysis showed
463 that high glucose treatment of ECs from diabetic mice resulted in the downregulation of Dab2
464 (Fig. 5B-C). Similar to the qPCR results, western blot analysis revealed significantly

465 downregulated FoxM1 protein levels in the diabetic group or high glucose treated group
466 compared to non-diabetic controls (Fig. 5D-G).

467 The concomitant downregulation of FoxM1 and Dab2 transcripts under diabetic conditions raises
468 the possibility that, as a regulatory transcription factor, FoxM1 directly influences Dab2
469 expression to modulate VEGFR2-mediated endothelial function. FoxM1 has been shown to
470 promote cell cycle progression, cell proliferation, and cellular metabolism[39,40], while Dab2 is a
471 critical regulator of VEGFR2 signaling. To investigate how FoxM1 regulates Dab2 expression
472 and VEGFR2 signaling, we used ChIP-qPCR analysis in ECs to determine if FoxM1 can bind to
473 the Dab2-promoter and other regulatory regions by using ChIP-qPCR analysis in ECs isolated
474 from wild type mice. We used the JASPAR database[41,42] to predict potential FoxM1 transcription
475 factor binding sites. A potential binding site within the promoter region of the Dab2 locus with
476 the highest score was selected for further study (Fig. 5H, S4A). ChIP-qPCR results showed that
477 indeed FoxM1 binds to this predicted region within the promoter region of Dab2 in ECs.
478 Interestingly, the binding of FoxM1 to the Dab2 promoter region is decreased when the ECs
479 were treated with high-concentration glucose or the FoxM1 inhibitor FDI-6 (Fig. 5I). More
480 importantly, disrupting the FoxM1 binding site with CRISPR/Cas-induced mutation in ECs also
481 significantly diminished FoxM1 binding. Our data demonstrate that FoxM1 directly binds to the
482 promoter region of Dab2 and disruption of this binding regulates its transcription.

483 **FoxM1 inhibitor FDI-6 downregulates Dab2 expression and the phosphorylation of**
484 **VEGFA-induced VEGFR2**

485 The significance of FoxM1 in ECs and vascular repair is underscored by its role in promoting
486 endothelial regeneration and resolving inflammatory lung injury. FoxM1, expressed during
487 embryogenesis in various cell types, including ECs, is crucial for pulmonary vascular ECs
488 proliferation and endothelial barrier recovery post-inflammatory injury. Notably, FoxM1
489 facilitates the reannealing of endothelial adheres junctions, enhancing endothelial barrier
490 function post-vascular injury. Aging-related impairment in endothelial regeneration and
491 inflammatory injury resolution is linked to inadequate FoxM1 induction, which, when addressed
492 through transgenic expression, improves outcomes in aged mice, highlighting the potential of
493 FoxM1 as a target for vascular repair interventions[43-46].

494 To determine if FoxM1 controls Dab2 transcription, we used the small molecule FDI-6 to
495 specifically inhibit FoxM1 function. FDI-6 is a FoxM1 transactivational inhibitor that blocks its
496 DNA binding[47,48]. Immunofluorescence staining of primary ECs revealed a significant decrease
497 in the expression of pVEGFR2 and Dab2 in FDI-6-treated conditions compared to the control
498 group, while the expression of FoxM1 remained unchanged (Fig 6A-C). In the VEGF signaling
499 pathway, ERK and AKT would normally be phosphorylated and activated. In high glucose
500 treatments, we observed diminished phosphorylation and activation of VEGFR2 (pVEGFR2),
501 Akt (pAkt), and ERK (pERK) (Fig. 6D-E). Furthermore, FDI-6 treatment reduced the protein
502 levels of pVEGFR2 as well as activation of both pERK and pAKT (Fig. 6F-G). In contrast, the
503 total protein level of FoxM1 was unaffected by FDI-6 treatment. These observations suggest that
504 FoxM1 regulates the expression of Dab2 which, in turn, controls VEGFR2 signaling.

505

Discussion

507 Chronic non-healing wounds in diabetes present a complex challenge and impaired angiogenesis
508 appears to underpin these defects in tissue repair and regeneration. Blunted angiogenesis is often
509 attributed to dysregulated signaling and aberrant gene expression precipitated by diabetic
510 conditions. Therefore, identifying crucial angiogenesis modulators is crucial to illustrate the
511 pathogenesis of blunted angiogenesis in diabetes and assess their therapeutic utility. Our
512 observations here provide important insights into the precise involvement of the highly
513 conserved endocytic adaptor protein, Dab2, and its transcriptional regulation during wound-
514 induced angiogenesis in diabetes. Dab2 is widely expressed in various tissues, suggesting tissue-
515 specific and context-dependent roles in multiple physiological processes[49]. Dab2 primarily
516 functions as a cytosolic, clathrin and cargo binding adaptor protein, with a pivotal role in
517 endocytosis. By facilitating the internalization of cargo molecules and the binding of clathrin-
518 coated vesicles to cargo proteins through clathrin-mediated endocytosis, Dab2 not only facilitates
519 signal transduction and receptor recycling but also plays a crucial role in maintaining cellular
520 homeostasis and regulating intracellular trafficking[50,51].

521 Intriguingly, Dab2 and its phosphorylated form are enriched in ECs[13,52]. Studies in *Xenopus* and
522 *Zebrafish* have revealed a functional contribution of Dab2 to developmental angiogenesis
523 through both VEGF-dependent and VEGF-independent mechanisms[53-56]. Earlier *in vitro* studies
524 revealed that Dab2 function is conducive to EC migration via mitigating VEGF signaling[49,57].
525 Similarly, Dab2 is required for the vascularization of the brain tissue and the establishment of the
526 neurovascular unit in part by enhancing VEGF signaling[58,59]. At least two other studies suggested
527 that activated receptor endocytosis through Dab2 results in augmented VEGF signaling in
528 ECs[14,56]. Nakayama *et al.* showed that phosphorylation of its phosphotyrosine-binding (PTB)
529 domain diminishes its interaction with the VEGF pathway receptors, VEGFR-2 and VEGFR-3,
530 revealing the specificity of Dab2 for VEGFRs[14].However, the upstream regulatory mechanisms
531 moderating the expression of Dab2 and its interaction with VEGFR2 remain unknown.
532 Furthermore, despite the well-established pro-angiogenic role of Dab2, the therapeutic potential
533 of exploiting Dab2 mediated angiogenesis to enhance wound healing in a disease context (*i.e.*,
534 diabetic wounds), has remained unexplored.

535 In our quest to investigate the involvement of endocytic adaptor proteins in mitigating aspects of
536 diabetes, we identified Dab2 via our bulk RNA-sequencing analysis of hyperglycemic ECs as
537 one of the downregulated genes. Similarly, we observed that ECs isolated from the STZ-induced
538 diabetic mice model, showed a significant downregulation of Dab2 mRNA and protein levels.
539 Although the precise involvement of Dab2 in diabetes remains to be addressed, Dab2 appears to
540 be involved in regulating blood glucose metabolism and its deficiency at least in myeloid cells,
541 has been implicated in compromised glucose tolerance in mice[60]. More intriguingly, and only
542 recently, polymorphisms in the Dab2 gene have been associated with type 2 Diabetes Mellitus
543 (T2DM) in a recent population-based study [55].

544   Because of the lack of information about the precise role of dab2 in diabetes, we went on to
545   develop an EC-specific Dab2-deficient mouse model to examine the effects of Dab2 deletion on
546   angiogenesis in diabetic conditions. we observed that endothelial-specific loss Dab2 was strongly
547   associated with delayed wound healing response and diabetic background further exacerbated
548   this process in Dab2-EC^{iKO} mice, coupled with severely blunted angiogenesis. Meanwhile our *in*
549   *vitro* model revealed that loss of endothelial Dab2 resulted in curtailed angiogenesis, as
550   evidenced by diminished cell migration, network formation, and proliferation.

551   Mechanistically, Dab2 deletion affected VEGFR2 activation, thereby impacting vascular
552   development both *in vitro* and *in vivo*. While the DPI, which blocked the certain domain that
553   Dab2 interact with VEGFR2, could downregulate the VEGF2 activation in VEGFA stimulated
554   ECs. These results align with prior studies on the role of Dab2 in angiogenesis but introduce
555   novel insights, including a comprehensive *in vivo* evaluation of angiogenesis in the diabetic
556   context. This unique approach enhances our understanding in dissecting the pathological
557   mechanisms of Dab2 underlying diabetic vascular complications.

558   Delayed wound healing in diabetic patients presents a significant clinical challenge while the
559   inhibitory effect of endothelial-specific Dab2 knockout on wound healing in our result suggested
560   that exogenous supplementation of Dab2 could be a potential therapeutic approach.
561   Consequently, we investigated the effects of exogenous Dab2 restoration on angiogenesis *in vivo*
562   and *in vitro*. In this study, we employed a novel method to administer Dab2 supplementation via
563   the deployment of *Dab2*-mRNA encapsulated in LNP conjugated with Lyp1 peptide. This novel
564   therapeutic approach bypasses common encumbrances associated with other modes of delivery,
565   such as inadequate absorption or shorter half-life of delivered proteins. Consistently, a recent
566   study has demonstrated the safety and specificity of augmenting VEGFA via nanoparticles[61].
567   The LNPs-Lyp1-Dab2 mRNA group exhibited significantly accelerated wound healing activity
568   compared with the untreated diabetic siblings, as observed by enhanced wound closure and
569   healing rates, with most wounds fully healed by day 7. This result demonstrated the feasibility
570   and positive effect of Dab2 mRNA supplementation *in vivo*. The beneficial effects of Dab2
571   restoration on angiogenesis also suggested that supplementation of Dab2 may serve as a possible
572   therapeutic target for diabetes patients delayed wound healing.

573   Further delving into the mechanism, we demonstrated that FoxM1, a highly conserved
574   transcription factor, exerts regulatory control over Dab2 expression in ECs during angiogenesis
575   associated with wound healing. Notably, we showed that FoxM1 binds to the Dab2 promoter to
576   drive Dab2 expression. Therefore, we have established that FoxM1 exerts a positive regulatory
577   control on Dab2 transcription, adding further insights into the molecular mechanisms regulating
578   angiogenesis during wound healing in diabetic conditions.

579   Although previous studies have suggested an involvement of FoxM1 in the pathogenesis of
580   diabetes, emerging studies have revealed that deletion of FoxM1 in diabetic mice impairs wound
581   healing, in part, via impeded recruitment of immune cells[62]. However, the endothelial-specific
582   role of FoxM1 in diabetic wounds was not addressed. FoxM1 plays a crucial role in β-cell
583   proliferation, essential for pancreatic repair and insulin secretion[63]. It activates pathways critical

for β-cell growth and interacts with regulatory genes, enhancing its transcriptional activity via the insulin receptor-mediated pathway. Additionally, FoxM1's involvement extends to nutrition-induced β-cell growth and its significance in gestational diabetes, highlighting its importance in β-cell function across various physiological conditions[61,63]. While previous studies acknowledge the pivotal role of FoxM1 in diabetes-related cellular functions and β-cell proliferation, our study delves into the mechanistic interaction between FoxM1 and Dab2 within the context of ECs and angiogenesis during wound healing in diabetic conditions.

Our study provides crucial insights into the role of Dab2 and FoxM1 in diabetic wound healing, highlighting the therapeutic potential of Dab2 mRNA encapsulated in lipid nanoparticles. This novel approach not only advances our understanding of the molecular mechanisms underlying diabetes-related angiogenesis and wound repair but also opens new avenues for developing targeted treatments for diabetic complications.

620   **Disclosures**

621   None.

622

623
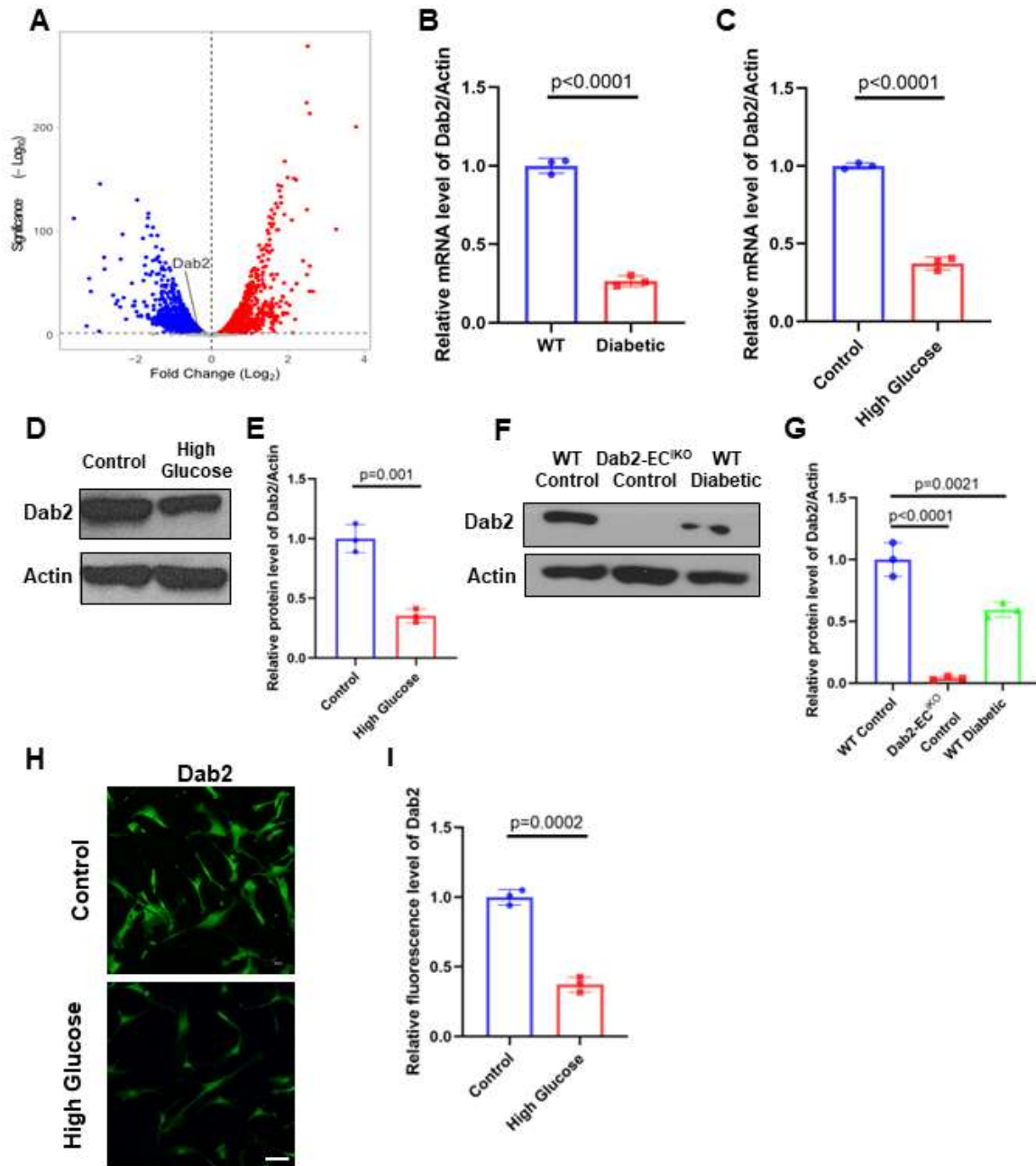
**Figure 1. Diabetes and high glucose treatment in ECs leads to the downregulation of Dab2.**

(A) Volcano plot of differentially expressed genes and in skin ECs cultured in high vs normal concentration of glucose for 48 hours. The x-axis shows the log2 fold change (log2FC) and the y-axis represents the negative logarithm of the p-value (-log10 p-value) (n = 3).

(B) RNA abundance of Dab2 in ECs isolated from normal or diabetic mice skin determined by qRT-PCR. (n = 3, results are presented as mean ± SD, p value calculated by t-test).

(C) RNA abundance of Dab2 in skin ECs cultured in normal or high concentration of glucose

631 determined by qRT-PCR. (n = 3, results are presented as mean ± SD, p value calculated by t-
632 test).

633 (D) Representative western blots of Dab2 in skin ECs cultured in normal (Control) or high
634 concentration of glucose

635 (E) Quantitation of protein level of Dab2 relative to Actin in (C). (n = 3, results are presented as
636 mean ± SD, p value calculated by t-test).

637 (F) Representative western blots of Dab2 in skin ECs isolated from WT control mice, Dab2-
638 EC^{iKO} control mice and diabetic mice.

639 (G) Quantitation of protein level of Dab2 relative to Actin in (E). (n = 3, results are presented as
640 mean ± SD, p value calculated by ANOVA).

641 (H) Representative immunofluorescence staining of Dab2 (green) in ECs treated with high or
642 normal concentration of glucose for 24 hours. Scale bar=50 μm

643 (I) Quantitation of fluorescence intensity in (H). (n = 3, results are presented as mean ± SD, p
644 value calculated by t-test).

645

646

647
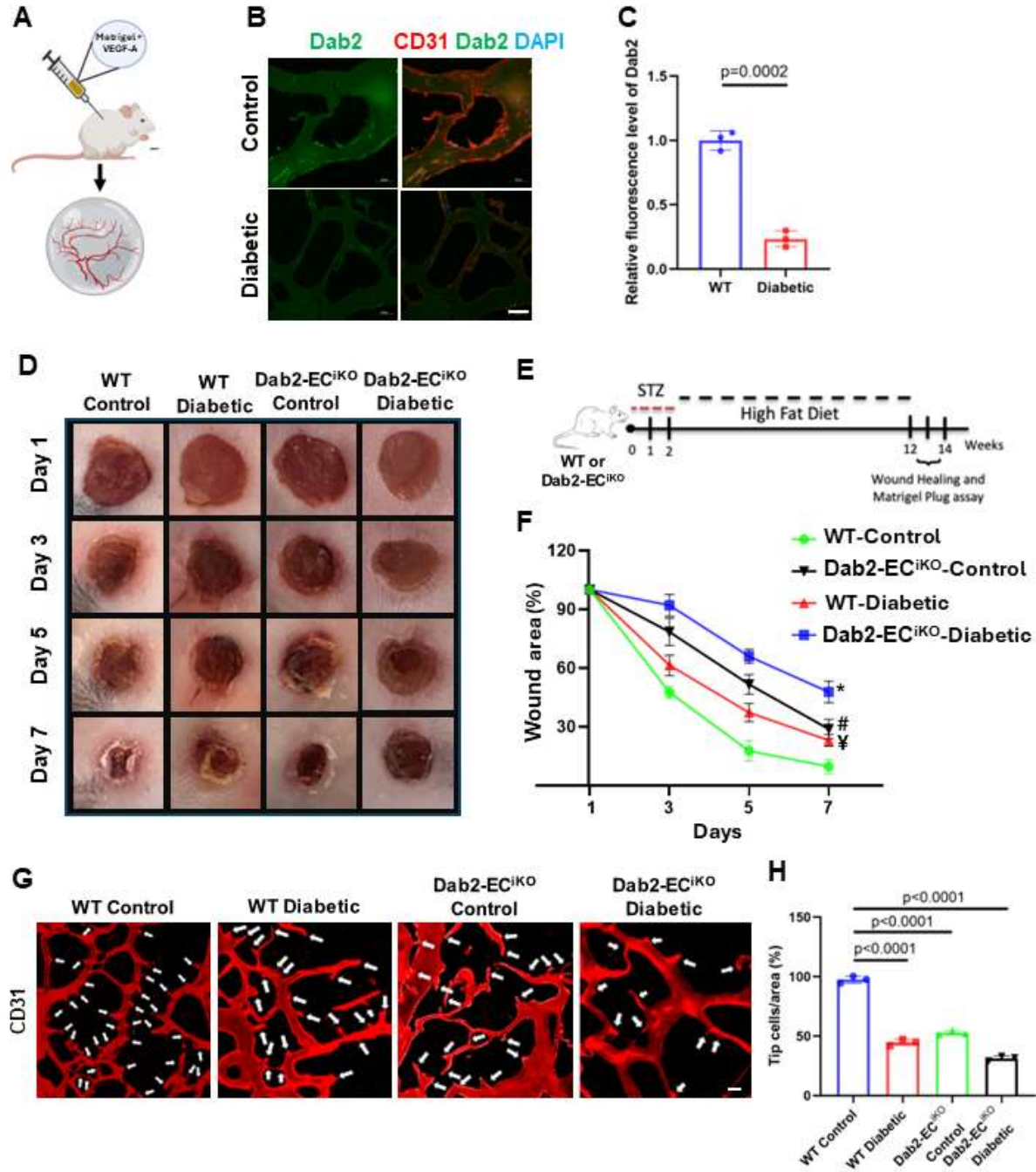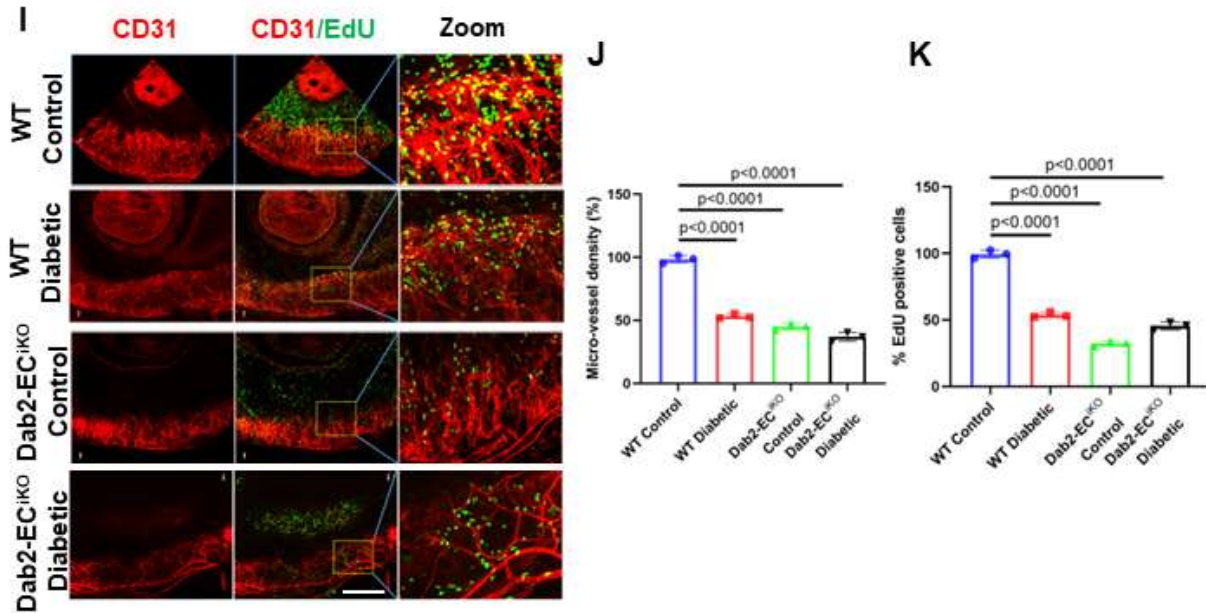
Figure 2. EC-specific Dab2 knockout cause reduced angiogenesis *in vivo*.

(A) Schematic diagram of the Matrigel plug assay

(B) Representative immunofluorescent staining of Dab2 (green) and CD31(red) in blood vessels in sections of Matrigel implant from WT and diabetic mice one week after injection. Scale bar=50μm.

(C) Quantitation of Dab2 fluorescence intensity in (B). (n = 3, results are presented as mean ± SD, p value calculated by t-test).

(D) Representative figures of wounds from wound healing assays in WT control mice, WT diabetes mice, Dab2-EC[iKO] control mice and Dab2-EC[iKO] diabetes mice.

(E) Schematic diagram of the protocol used to induce diabetes in mice for the wound healing assay that illustrates the step-by-step treatment process, starting with the administration of STZ followed by a high-fat diet regimen.

(F) Analysis of wound closure conducted at 1, 3, 5, and 7 days after the initial wound creation, providing a timeline view of the healing process (*P < 0.05 vs. WT mice; #P<0.05 vs. WT mice; ¥P < 0.05 vs. WT mice. n = 6, results are presented as mean ± SD, p value calculated by ANOVA)

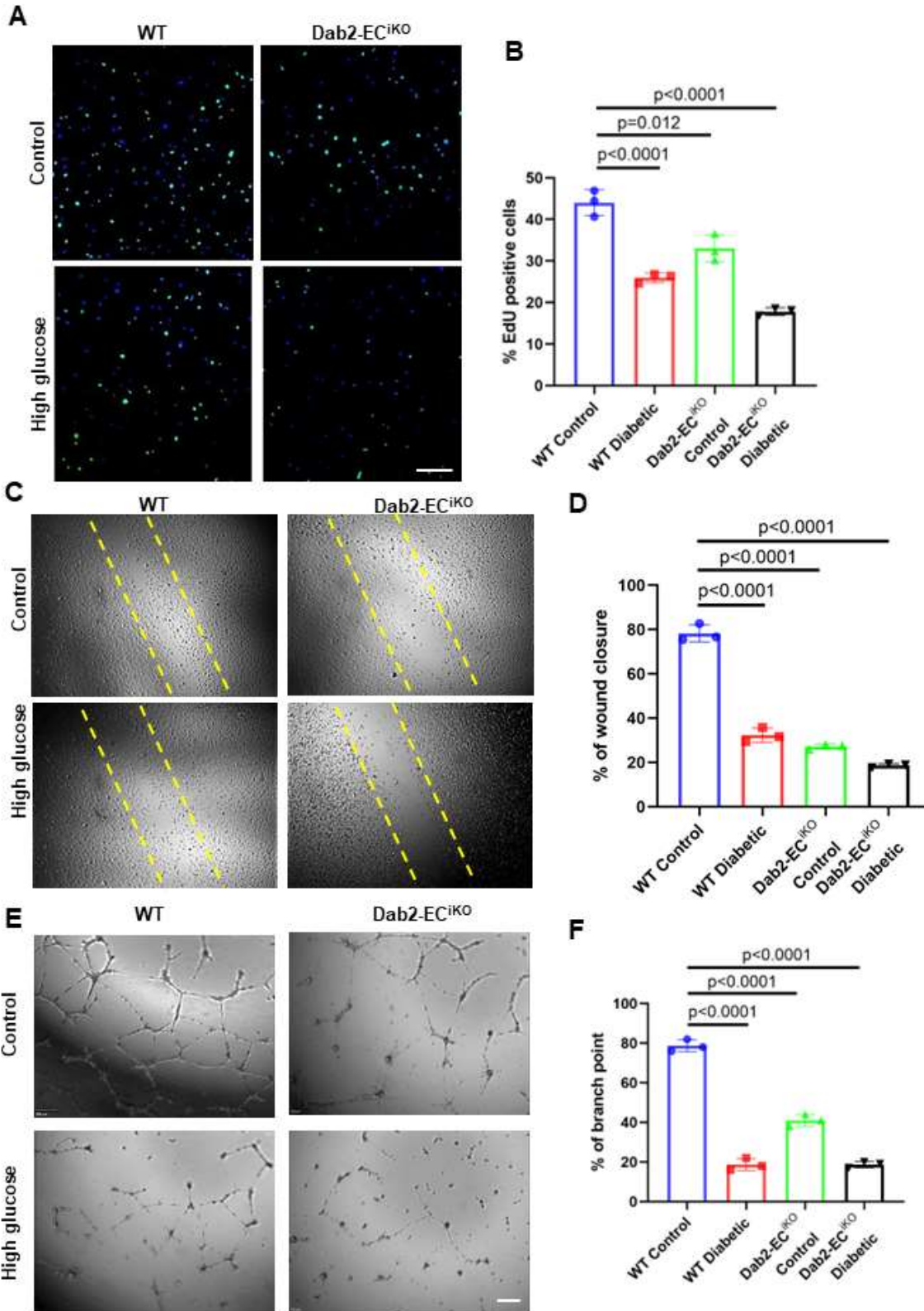(G) Representative immunofluorescence staining of cryosections of Matrigel plugs. Scale bar=50μm.

(H) Quantitation of CD31-positive tip cell percentage in (F). (n = 3, results are presented as mean ± SD, p value calculated by ANOVA).

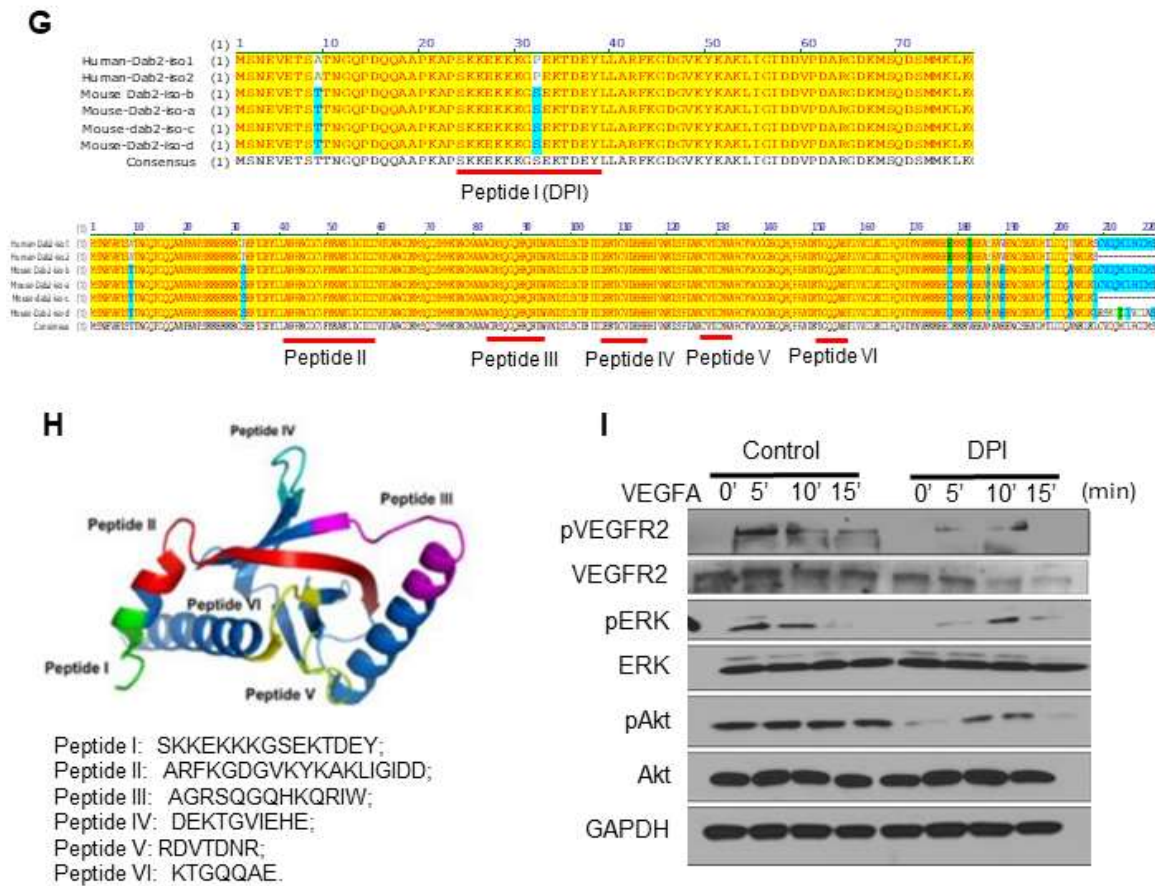(I) Retinal micropocket assay to assess the effect of diabetes and Dab2 deletion on angiogenesis. Scale bar=500μm.

(J) Quantification of the density of the blood vessels. (n = 3, results are presented as mean ± SD, p value calculated by ANOVA).

672 (K) Quantification of the density of EdU-positive proliferative cells. (n = 3, results are presented
673   as mean ± SD, p value calculated by ANOVA).

674

675

G

Peptide I (DPI)

Peptide II   Peptide III   Peptide IV   Peptide V   Peptide VI

H

Peptide IV
Peptide III
Peptide II
Peptide VI
Peptide I
Peptide V

Peptide I: SKKEKKKGSEKTDEY;
Peptide II: ARFKGDGVKYKAKLIGIDD;
Peptide III: AGRSQGQHKQRIW;
Peptide IV: DEKTGVIEHE;
Peptide V: RDVTDNR;
Peptide VI: KTGQQAE.

I

	Control				DPI				
VEGFA	0'	5'	10'	15'	0'	5'	10'	15'	(min)

pVEGFR2
VEGFR2
pERK
ERK
pAkt
Akt
GAPDH

Figure 3. EC-specific Dab2 knockout cause reduced angiogenesis *in vitro*.

(A) Representative figures of EdU incorporation (green) in WT skin ECs cultured in normal or high concentration of glucose and skin ECs from Dab2-EC[iKO] mice with or without high concentration of glucose. Scale bar=200μm

(B) Quantitation of the proportion of EdU-positive cells in (A). (n = 3, results are presented as mean ± SD, p value calculated by ANOVA).

(C) Representative figures of wound closure scratch assay of ECs monolayers as described in (A).

(D) Quantitation of wound closure results in (C). (n = 3, results are presented as mean ± SD, p value calculated by ANOVA).

(E) Representative figures of tube formation assay of cells as described in (A).

(F) Quantitation of branch points in results from (E). (n = 3, results are presented as mean ± SD, p value calculated by ANOVA).

(G) Alignment of human, rat, and mouse Dab1 and Dab2 protein-coding sequences, identifying a consistent RGD motif and an additional KGD motif in the Dab2 PTB domain, suggesting evolutionarily conserved integrin binding capabilities.

(H) The presence of an RGD peptide motif and an additional KGD motif in the Dab2 PTB

694   domain suggests integrin binding capabilities.

695   (I) Immunoblot of VEGFR2-proximal signaling components in skin ECs pretreated with DPI

696   followed by VEGFA stimulation.

697
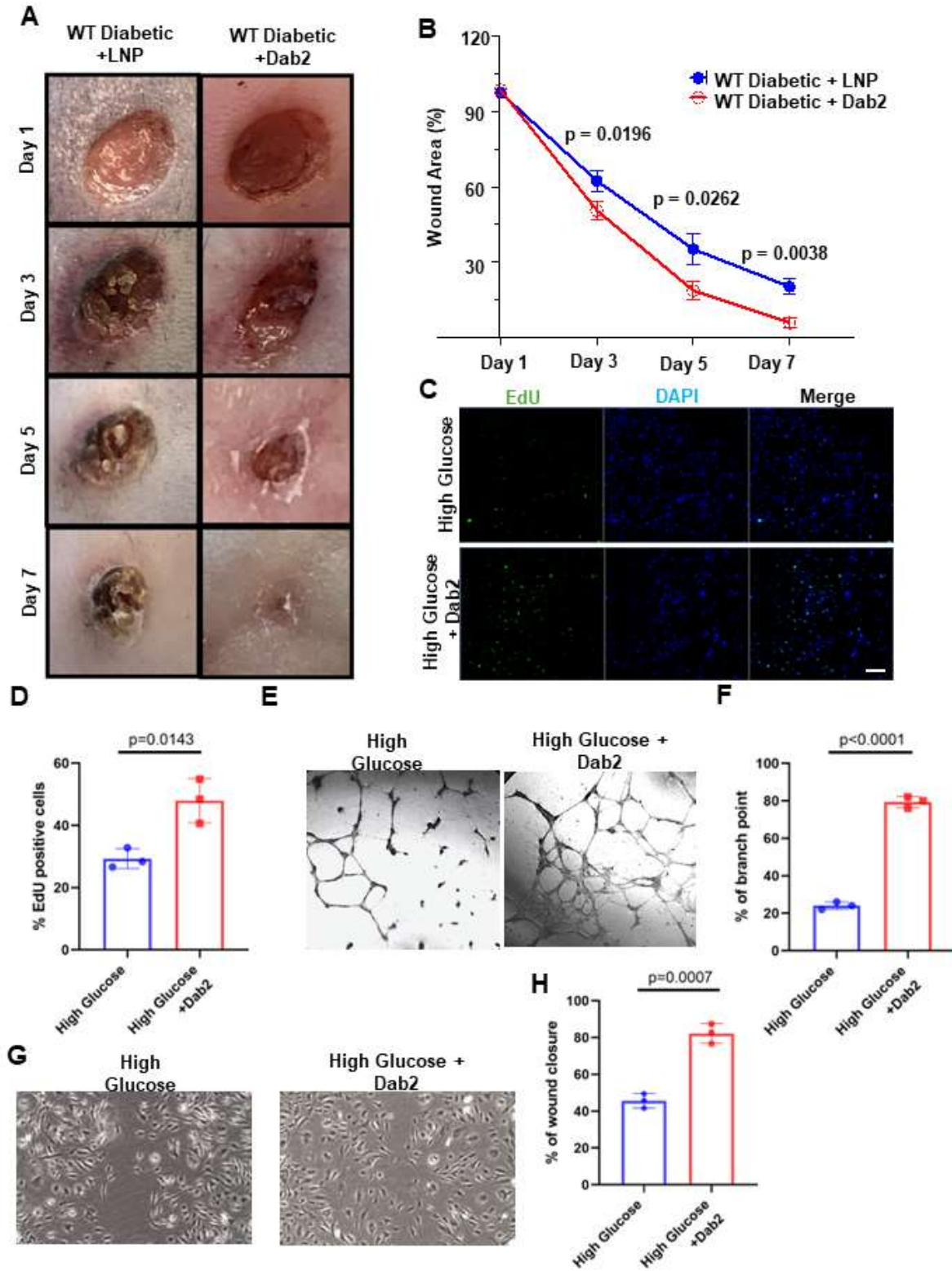
Figure 4. Restoration of Dab2 expression in ECs rescues impaired angiogenesis and wound healing in diabetic mice.

701 (A) Representative figures of wounds from wound healing assays in diabetic mice treated with
702   LNPs carrying mRNAs encoding GFP or Dab2.
703 (B) Quantitation of wound closure conducted on day 1, 3, 5, and 7 after the initial wound (n=5, p
704   value calculated using t-test).
705 (C) Representative figures of EdU of skin ECs cultured in high concentration of glucose infected
706   with empty lentivirus vector or lentivirus carrying Dab2 cDNA. Scale bar=200μm.
707 (D) Quantitation of the proportion of EdU-positive cells in (C). (n=3, p value calculated using t-
708   test).
709 (E) Representative figures of tube formation assay on skin ECs cultured in high concentration of
710   glucose and infection empty vector or lentivirus carrying Dab2 cDNA.
711 (F) Quantitation of branch points in results from (E). (n = 3, results are presented as mean ± SD,
712   p value calculated by t-test).
713 (G) Representative figures of wound healing assay on skin ECs cultured in high concentration of
714   glucose and infection empty vector or lentivirus carrying Dab2 cDNA.
715 (H) Quantitation of wound closure results in (G). (n = 3, results are presented as mean ± SD, p
716   value calculated by t-test).

717
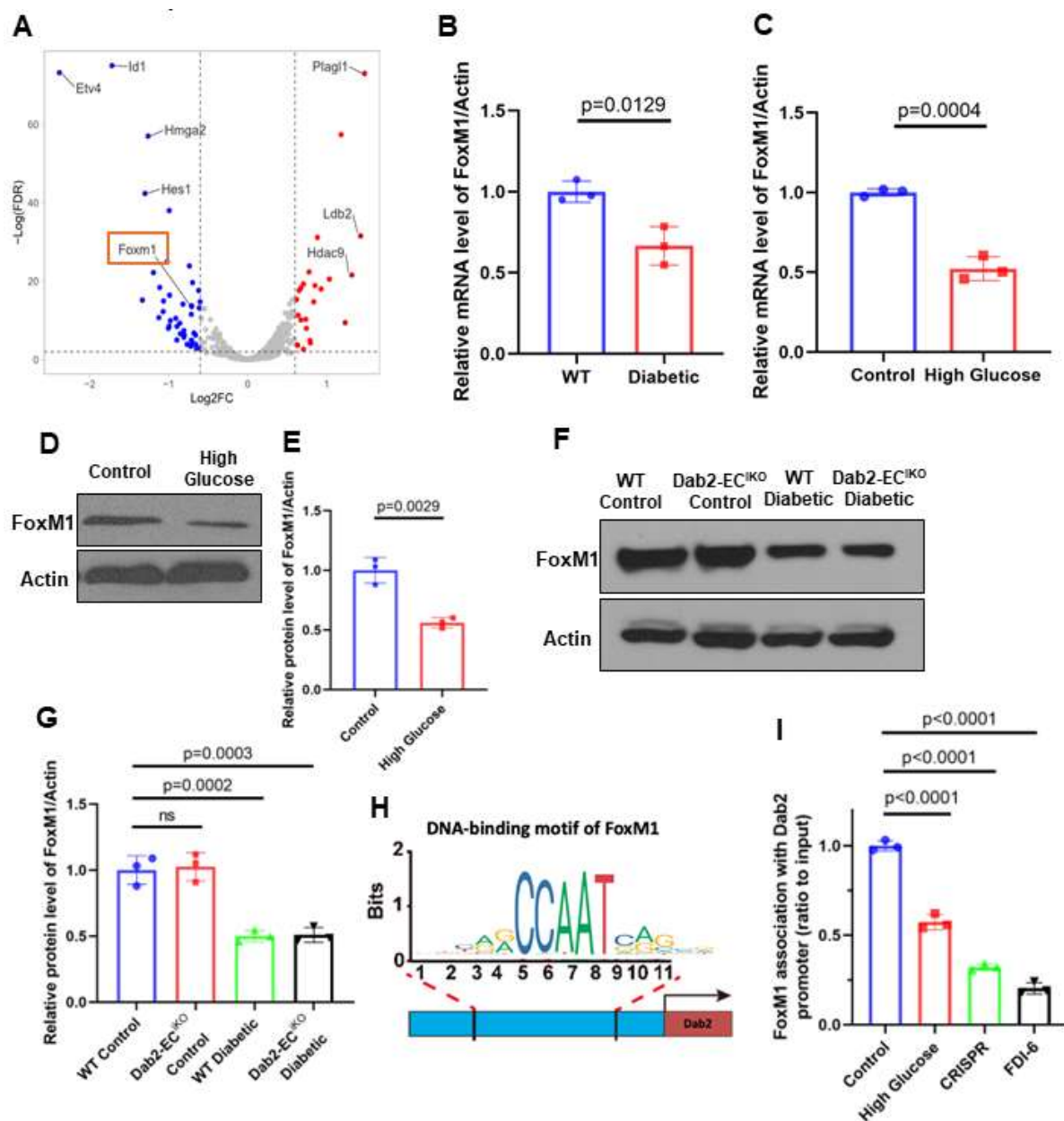
Figure 5. Foxm1 is downregulated in diabetes and regulates Dab2 transcription.

(A) Volcano plot of differentially expressed transcription factors in skin ECs cultured in high vs normal concentration of glucose for 24 hours. The x-axis shows the log2 fold change (log2FC) and the y-axis represents the negative logarithm of the p-value (-log10 p-value). n = 3.

(B) RNA abundance of Foxm1 in ECs isolated from normal or diabetic mice skin determined by qRT-PCR. (n = 3, results are presented as mean ± SD, p value calculated by t-test).

(C) RNA abundance of Foxm1 in skin ECs cultured in normal or high concentration of glucose determined by qRT-PCR. (n = 3, results are presented as mean ± SD, p value calculated by t-

728   test).

729   (D) Representative western blots of Dab2 in skin ECs cultured in control or high concentration of

730   glucose.

731   (E) Quantitation of protein level of Dab2 relative to Actin in (D). (n = 3, results are presented as

732   mean ± SD, p value calculated by t-test).

733   (F) Representative western blots of Dab2 in skin ECs isolated from WT control mice, Dab2-

734   EC^{iKO} control mice, WT diabetic mice and Dab2-EC^{iKO} diabetic mice.

735   (G) Quantitation of protein level of Dab2 relative to Actin in (E). (n = 3, results are presented as

736   mean ± SD, p value calculated by t-test).

737   (H) JASPAR-predicted FoxM1-Binding site in the Dab2 promoter.

738   (I) FOXM1 binding to the Dab2 promoter in ECs exposed to high concentration of glucose, or

739   FDI-6, or with a CRISPR-mediated deletion mutation in the FoxM1 binding site on the Dab2

740   promoter. (n = 3, results are presented as mean ± SD, p value calculated by ANOVA).

741

742
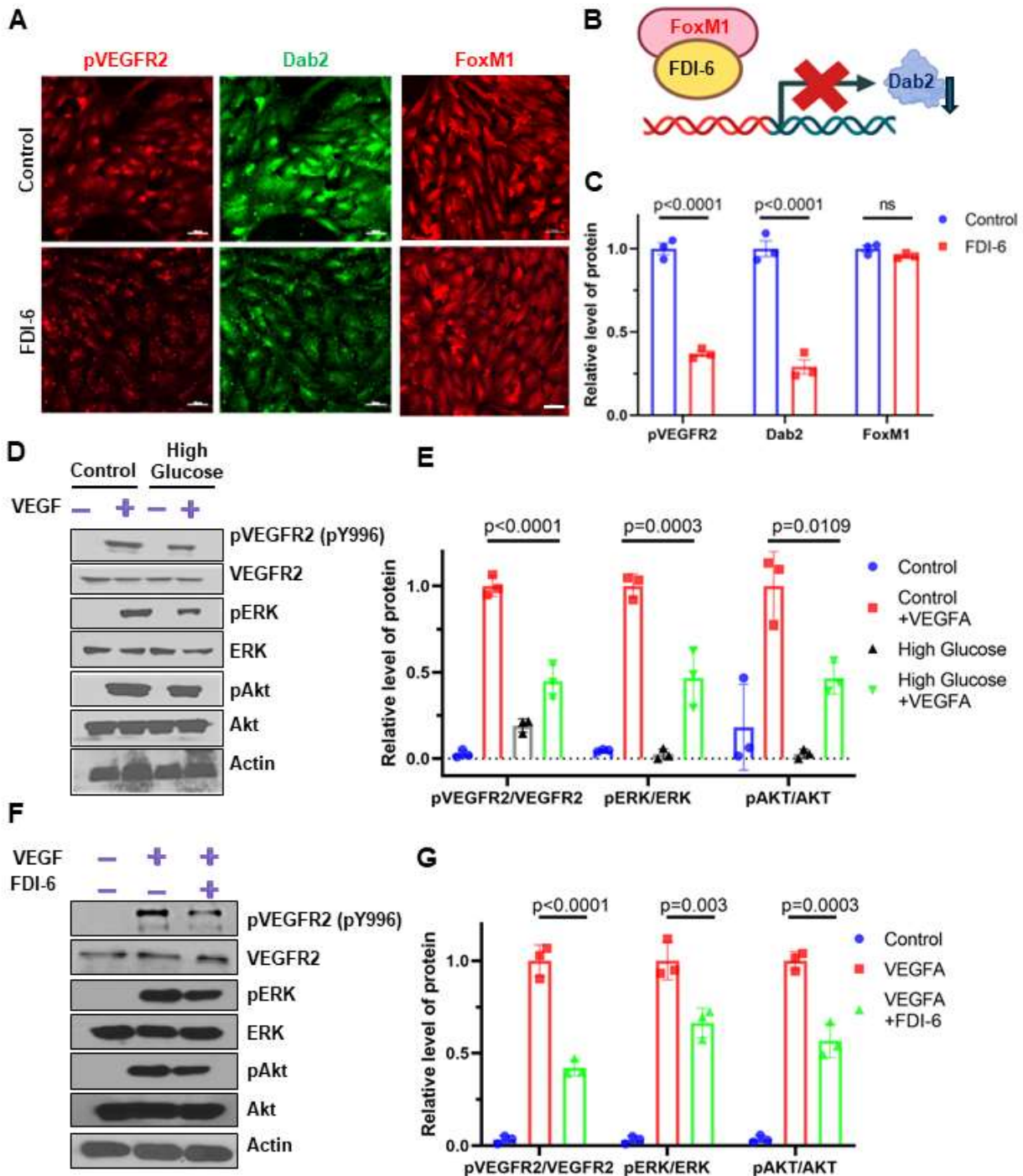
Figure 6. Foxm1 inhibitor FDI-6 downregulates Dab2 expression and the phosphorylation of VEGFA-induced VEGFR2.

(A) Representative immunofluorescence staining of skin ECs treated with or without FDI-6. Scale bar=50 μm.

(B) Schematic diagram showing inhibition of Dab2 expression by FDI-6

748 (C) Quantitation of the immunofluorescence intensity in (A). (n = 3, results are presented as

749   mean ± SD, p value calculated by t-test).

750 (D) VEGFA-induced phosphorylation of key VEGFR2-proximal signaling components in skin

751   ECs treated in control or high glucose concentration with or without VEGF assessed by

752   Western blot analysis.

753 (E) Quantitation of results described in (D). (n = 3, results are presented as mean ± SD, p value

754   calculated by ANOVA).

755 (F) Representative of Western blot of VEGFA-induced key VEGFR2-proximal signaling in skin

756   ECs treated with or without FDI-6.

757 (G) Quantitative analysis of immunoblots in (C). (n = 3, results are presented as mean ± SD, p

758   value calculated by ANOVA).

759
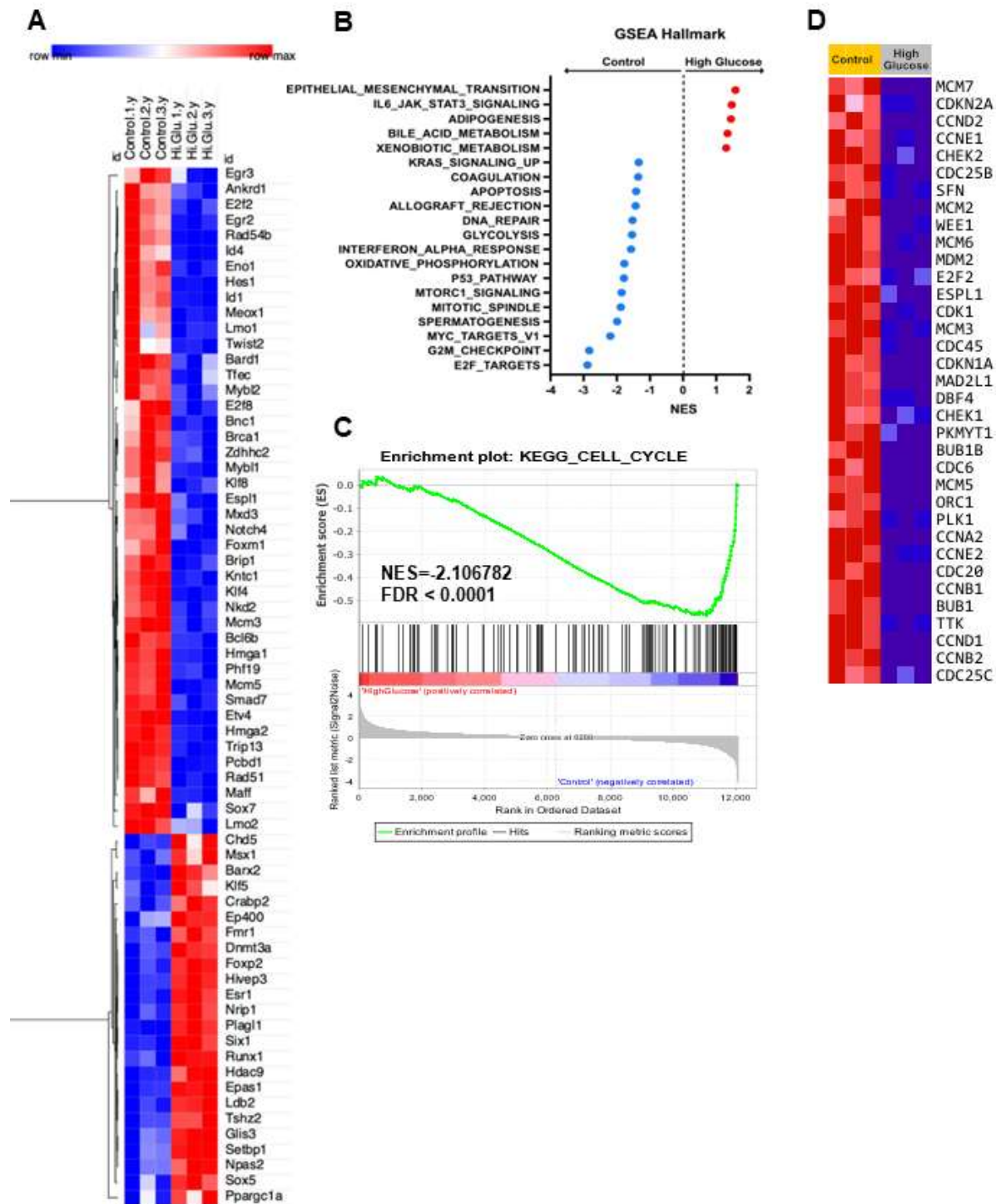
Figure S1. Heatmaps showing differentially regulated gene expression in CD31-enriched primary mouse skin ECs exposed to normal or high glucose concentrations for 48 hours.

(A) Differential gene expression analysis revealed 168 significantly downregulated and 386 significantly up-regulated genes in the ECs grown in high glucose culture conditions

765   compared to ECs cultured in normal glucose media. Sample genes are shown (n = 3).

766   (B) GSEA Hallmark genesets enriched on differentially expressed genes from bulk RNA-seq data

767   described in bulk RNA-sequencing. Geneset with a nominal p-value <0.05 and FDR <0.25

768   were included. Normalized Enrichment Score (NES) for all gene sets are shown.

769   (C) Enrichment plot for KEGG Cell Cycle.

770   (D) Multiple down-regulated genes in the high-glucose treatment group are involved in the

771   regulation of cell cycle progression (n = 3).

772

773
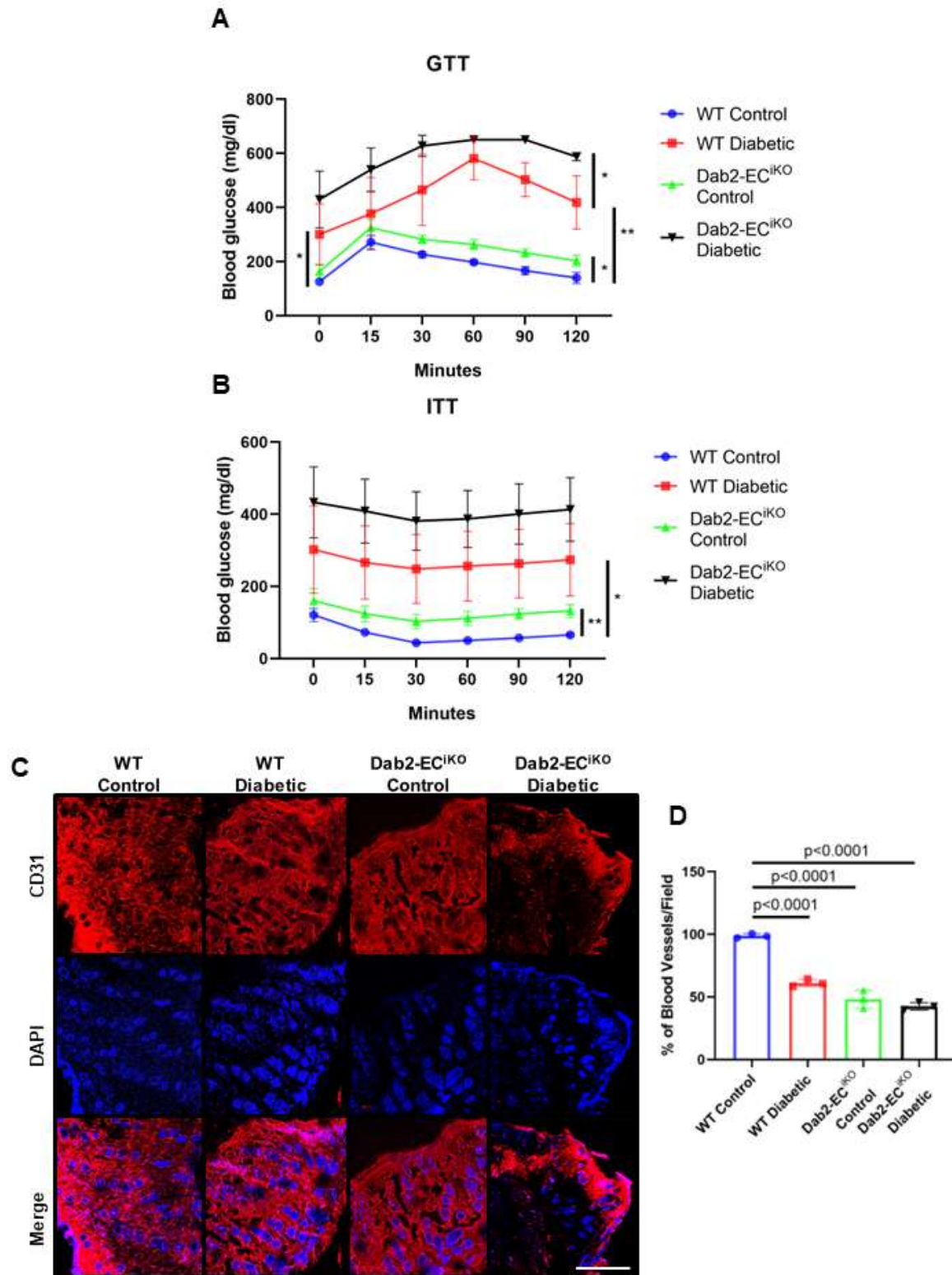
Figure S2. GTT and ITT of HFD WT mice and Dab2-EC^{iKO} mice, and wound CD31 in diabetic WT mice and Dab2-EC^{iKO} mice.

776   (A) Glucose tolerance test (GTT) of WT and Dab2-EC^{iKO} mice with or without diabetes after
777   low-dose STZ injection and 12-weeks HFD feeding described in Figure 2E. (n = 3-6, results
778   are presented as mean ± SD, p value calculated by Student's t-test, *p<0.05, **p<0.01).
779   (B) Insulin tolerance test (ITT) of WT and Dab2-EC^{iKO} mice with or without diabetes after low-
780   dose STZ injection and 12-weeks HFD feeding described in Figure 2E. (n = 5, results are
781   presented as mean ± SD, p value calculated by Student's t-test, *p<0.05, **p<0.01).
782   (C) Representative immunofluorescence staining of CD31 (red) in wound area from collected in
783   mice described in Figure 2D. Scale bar=100μm.
784   (D) Quantitation of CD31-positive blood vessel density in Figure 2D. (n = 3, results are
785   presented as mean ± SD, p value calculated by ANOVA).

786

787
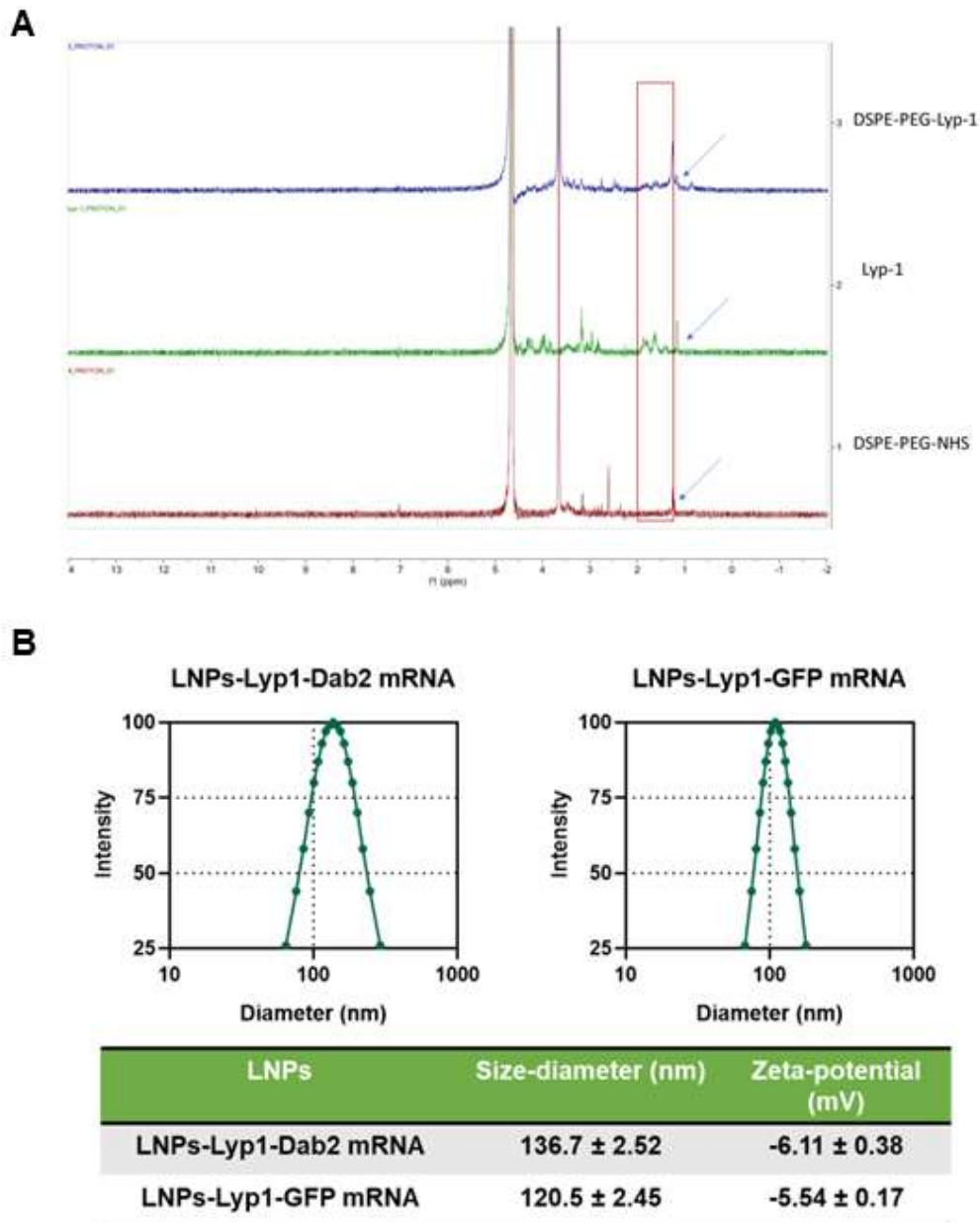
Figure S3. Characterization of the Lyp1-LNP-Dab2 mRNA- and Lyp1-LNP-GFP mRNA-containing lipid nanoparticles (LNPs).

(A) ^{1}H-NMR to characterize the successful synthesis of DSPG-PEG-Lyp1.

(B) Size and Zeta potential of LNPs-Lyp1-Dab2 mRNA and LNPs-Lyp1-GFP mRNA (control group).

A

794
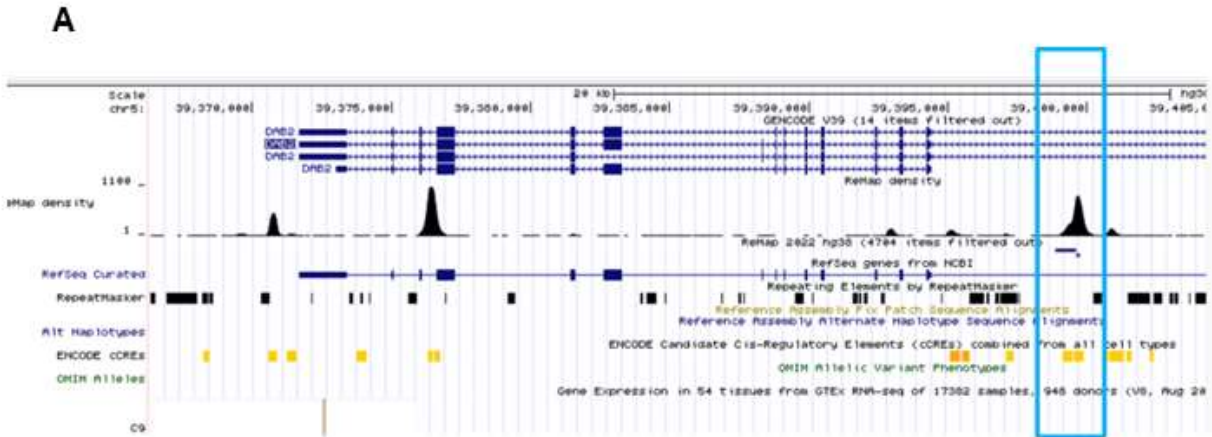
Figure S4. FoxM1 binding zone in Dab2 promoter.

(A) UCSC genome viewer display of FoxM1 binding sites (boxed peak) in Dab2 promoter region. The x-axis represents the genomic region of the Dab2 promoter, the y-axis shows the peak height of the FoxM1 binding sites.

799

Interaction residues of Fibromodulin to form H-bonds		Interaction residues of AXL to form H-bonds	
Predicted residues in Dab2(IP3R)	Frequency to form H-bonds	Predicted residues in VEGFR2	Frequency to form H-bonds
E33	21	R1027	27
K49	17	K1023	15
Q153	17	R1126	15
W37	16	D1129	14
M32	16	R819	13
Q88	12	R1022	11
E156	11	H816	11
K108	11	Y996	11
R42	10	R1172	10
N131	10	E815	9
Q154	10	K826	9
Y38	9	1170	9
R92	9	R1080	9
Q86	9	D1046	8
R132	9	N933	8
K44	8	H1173	7
T35	8	H891	6
H89	7	R932	6
R84	7	Q1149	6
E113	7	E1146	5
K108	7	E1134	5
I57	7	D1171	5
R126	6	Y1082	5
D106	5	Q1137	4
Q91	5	935	4
D164	5	L995	4
T109	5	Y1130	4
D59	4	R1061	3
D161	4	D1028	3
Y50	4	E993	3
K34	4	R1124	3
E115	4	D1141	3
Q145	4	D994	3
Q143	4	D823	3
K163	3	R880	3
H114	3	I1025	3

D66	3	G1122	3
K90	3	H1159	2
D46	3	E1155	2
K51	3	Q1085	2
T129	3	E1158	2
G87	3	Y1054	2
S85	3	R1066	2
K53	2	H894	2
K75	2	Y938	2
K77	2	Y1136	2
K150	2	R1118	2
R64	2	R1022	2
Q91	2	Y822	1
Q167	2	H1026	1
		D1064	1
		R1051	1
		R1052	1
		K1120	1
		E815	1
		E1017	1
		R1051	1
		R1052	1
		K997	1
		K1070	1

Table 1. Interacting residues between mouse Dab2 (2LSW) and VEGFR2

The crystal structure of mouse Dab2 (PDB ID: IP3R) and VEGFR2 were taken from the PDB database and used to perform the docking experiments using ClusPro 2.0. There are total 200 models per each docking experiment. The frequency of residues in Dab2 and VEGFR2 to form H-bonds among these models were ranked, respectively. From the modeling, the E33, K49, Q153, E37, and Q88 residues from Dab2 and the R1027, K1023, R1126, D1129, R819, R1022, H816, and Y996 residues from VEGFR2 were critical to form the complex.

Gene	Forward primer	Reverse primer
Kdr (VEGFR2)	5'- ATCCACTGGTATTGGCAGT - 3'	5'- AGGTGCCCAGGAAAAGACGA - 3'
Dab2	5'- CCCAGCAGTACAAGTCTGGA - 3'	5'- AGGACTGAGTGGACATGGTG - 3'
FoxM1	5'- ACCATAGCAACCCTAGCAGC - 3'	5'- GGGTACCACAGGATGAAAGCA - 3'
Ets1	5'- ACGCTGCATCCTATCAGCTC - 3'	5'- CGAGTTTACCACGACTGGCT - 3'
GATAd1	5'- GCAAGATGGGAAGCCGTACT - 3'	5'- GACTGGCGAGGGTAGGAATG - 3'
GAPDH	5'- GTCTCCTCTGACTTCAACAGCG - 3'	5'- ACCACCCTGTTGCTGTAGCCAA - 3'
B-Actin	5'- AGAGCTACGAGCTGCCTGAC - 3'	5'- AGCACTGTGTTGGCGTACAG - 3'

808 **Table S1. The list of primers used in qRT-PCR.**

809

Target antigen	Vendor or Source	Catalog #	Applications	Source Isotype	Cross activity
VEGFR2	Cell signaling	9698	WB	Rabbit	H M R
phospho-VEGFR2	Cell signaling	2478	WB/IF	Rabbit	H M
ERK	Cell signaling	4695	WB	Rabbit	H M R
phospho-ERK	Cell signaling	9106	WB	Mouse	H M R
Akt	Cell signaling	9272	WB	Rabbit	H M R
phospho-Akt	Cell signaling	4058	WB	Rabbit	H M R
Dab2	Santa Cruz	sc-136964	WB/IF	Mouse	H M
FoxM1	GeneTex	GTX100276	WB/IF	Rabbit	H M
Actin	Santa Cruz	sc-58673	WB	Mouse	H M R
GAPDH	Santa Cruz	sc-137179	WB	Mouse	H M R
Anti-Mouse IgG (H+L) Secondary Antibody, HRP	Thermo Fisher Scientific	31430	WB	Goat	M
Anti-Rabbit IgG (H+L) Secondary Antibody, HRP	Thermo Fisher Scientific	31460	WB	Goat	R
CD31	Thermo Fisher	BDB550274	IF	Rat	H M R
Alexa Fluor 488 anti-Rat (H+L)	Invitrogen	A-21208	IF	Donkey	Rat
Alexa Fluor 488 anti-Mouse (H+L)	Invitrogen	A-21202	IF	Donkey	M
Alexa Fluor 488 anti-Rabbit (H+L)	Invitrogen	A-21206	IF	Donkey	R
Alexa Fluor 594 anti-Rat (H+L)	Invitrogen	A-21209	IF	Donkey	Rat
Alexa Fluor 594 anti-Mouse (H+L)	Invitrogen	A-21203	IF	Donkey	M
Alexa Fluor 594 anti-Rabbit (H+L)	Invitrogen	A-21207	IF	Donkey	R

810 **Table S2. The list of antibodies.**

811

812

813
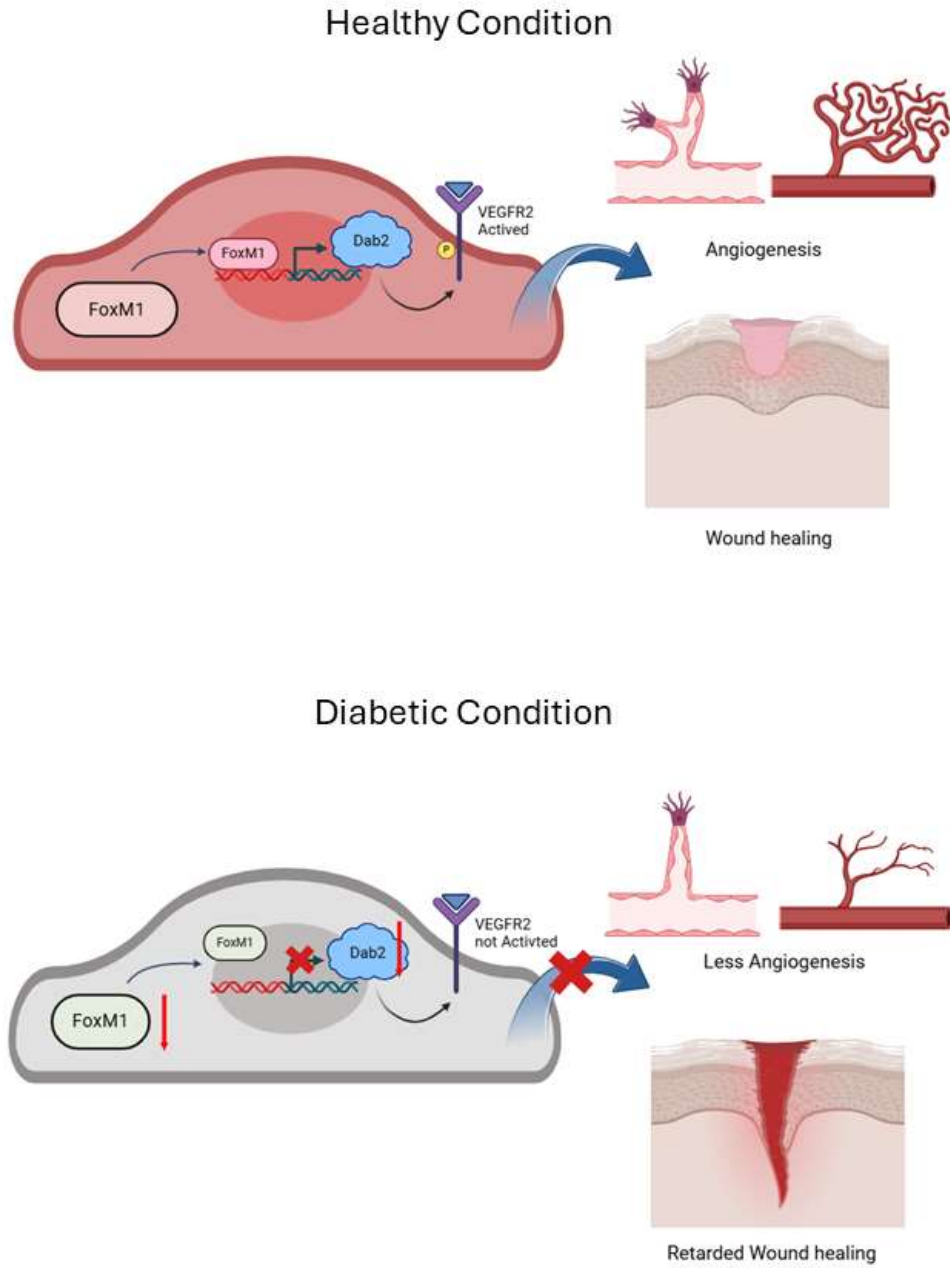
References

1   Driver, V. R., Fabbi, M., Lavery, L. A. & Gibbons, G. The costs of diabetic foot: the economic case for the limb salvage team. *J Am Podiatr Med Assoc* **100**, 335-341, doi:10.7547/1000335 (2010).

2   Boulton, A. J., Vileikyte, L., Ragnarson-Tennvall, G. & Apelqvist, J. The global burden of diabetic foot disease. *Lancet* **366**, 1719-1724, doi:10.1016/S0140-6736(05)67698-2 (2005).

3   Dixon, D. & Edmonds, M. Managing Diabetic Foot Ulcers: Pharmacotherapy for Wound Healing. *Drugs* **81**, 29-56, doi:10.1007/s40265-020-01415-8 (2021).

4   Veith, A. P., Henderson, K., Spencer, A., Sligar, A. D. & Baker, A. B. Therapeutic strategies for enhancing angiogenesis in wound healing. *Advanced Drug Delivery Reviews* **146**, 97-125, doi:10.1016/j.addr.2018.09.010 (2019).

5   Tonnesen, M. G., Feng, X. & Clark, R. A. Angiogenesis in wound healing. *J Investig Dermatol Symp Proc* **5**, 40-46, doi:10.1046/j.1087-0024.2000.00014.x (2000).

6   Nissen, N. N. *et al.* Vascular endothelial growth factor mediates angiogenic activity during the proliferative phase of wound healing. *Am J Pathol* **152**, 1445-1452 (1998).

7   Neufeld, G., Tessler, S., Gitay-Goren, H., Cohen, T. & Levi, B.-Z. Vascular endothelial growth factor and its receptors. *Progress in Growth Factor Research* **5**, 89-97, doi:10.1016/0955-2235(94)90019-1 (1994).

8   Koch, S., Tugues, S., Li, X., Gualandi, L. & Claesson-Welsh, L. Signal transduction by vascular endothelial growth factor receptors. *Biochem J* **437**, 169-183, doi:10.1042/BJ20110301 (2011).

9   Shibuya, M. Vascular endothelial growth factor and its receptor system: physiological functions in angiogenesis and pathological roles in various diseases. *J Biochem* **153**, 13-19, doi:10.1093/jb/mvs136 (2013).

10   Rivard, A. *et al.* Rescue of diabetes-related impairment of angiogenesis by intramuscular gene therapy with adeno-VEGF. *Am J Pathol* **154**, 355-363, doi:10.1016/S0002-9440(10)65282-0 (1999).

11   Warren, C. M., Ziyad, S., Briot, A., Der, A. & Iruela-Arispe, M. L. A ligand-independent VEGFR2 signaling pathway limits angiogenic responses in diabetes. *Sci Signal* **7**, ra1, doi:10.1126/scisignal.2004235 (2014).

12   Fadini, G. P., Albiero, M., Bonora, B. M. & Avogaro, A. Angiogenic Abnormalities in Diabetes Mellitus: Mechanistic and Clinical Aspects. *J Clin Endocrinol Metab* **104**, 5431-5444, doi:10.1210/jc.2019-00980 (2019).

13   Jing, Z., Jia-Jun, W. & Wei-Jie, Y. Phosphorylation of Dab2 is involved in inhibited VEGF-VEGFR-2 signaling induced by downregulation of syndecan-1 in glomerular endothelial cell. *Cell Biol Int* **44**, 894-904, doi:10.1002/cbin.11288 (2020).

14   Nakayama, M. *et al.* Spatial regulation of VEGF receptor endocytosis in angiogenesis. *Nat Cell Biol* **15**, 249-260, doi:10.1038/ncb2679 (2013).

15   Liao, G. B. *et al.* Regulation of the master regulator FOXM1 in cancer. *Cell Commun Signal* **16**, 57, doi:10.1186/s12964-018-0266-6 (2018).

16   Yang, Y., Zhang, B., Yang, Y., Peng, B. & Ye, R. FOXM1 accelerates wound healing in diabetic foot ulcer by inducing M2 macrophage polarization through a mechanism involving SEMA3C/NRP2/Hedgehog signaling. *Diabetes Res Clin Pract* **184**, 109121, doi:10.1016/j.diabres.2021.109121 (2022).

17   Roh, V. *et al.* The transcription factor FOXM1 regulates the balance between proliferation and aberrant differentiation in head and neck squamous cell carcinoma. *J Pathol* **250**, 107-119, doi:10.1002/path.5342 (2020).

18   Zhang, W. *et al.* FOXM1D potentiates PKM2-mediated tumor glycolysis and angiogenesis. *Mol Oncol* **15**, 1466-1485, doi:10.1002/1878-0261.12879 (2021).

19   Wu, H. *et al.* Epsin deficiency promotes lymphangiogenesis through regulation of VEGFR3 degradation in diabetes. *J Clin Invest* **128**, 4025-4043, doi:10.1172/JCI96063 (2018).

20   Conchinha, N. V. *et al.* Protocols for endothelial cell isolation from mouse tissues: brain, choroid, lung, and muscle. *STAR Protoc* **2**, 100508, doi:10.1016/j.xpro.2021.100508 (2021).

21   Xiong, L., McCoy, M., Murtazina, R., Podrez, E. A. & Byzova, T. V. Timely Wound Healing Is Dependent on Endothelial but Not on Hair Follicle Stem Cell Toll-Like Receptor 2 Signaling. *J Invest Dermatol* **142**, 3082-3092 e3081, doi:10.1016/j.jid.2022.04.018 (2022).

22   Birsner, A. E., Benny, O. & D'Amato, R. J. The corneal micropocket assay: a model of angiogenesis in the mouse eye. *J Vis Exp*, doi:10.3791/51375 (2014).

23   Dong, Y. *et al.* Targeting Epsins to Inhibit Fibroblast Growth Factor Signaling While Potentiating Transforming Growth Factor-beta Signaling Constrains Endothelial-to-Mesenchymal Transition in Atherosclerosis. *Circulation* **147**, 669-685, doi:10.1161/CIRCULATIONAHA.122.063075 (2023).

24   Uchida, M. *et al.* Protein cage nanoparticles bearing the LyP-1 peptide for enhanced imaging of macrophage-rich vascular lesions. *ACS Nano* **5**, 2493-2502, doi:10.1021/nn102863y (2011).

25   Song, N., Zhao, L., Zhu, M. & Zhao, J. Recent progress in LyP-1-based strategies for targeted imaging and therapy. *Drug Deliv* **26**, 363-375, doi:10.1080/10717544.2019.1587047 (2019).

26   Tuma, J. *et al.* Lipid Nanoparticles Deliver mRNA to the Brain after an Intracerebral Injection. *Biochemistry* **62**, 3533-3547, doi:10.1021/acs.biochem.3c00371 (2023).

27   Hassett, K. J. *et al.* Optimization of Lipid Nanoparticles for Intramuscular Administration of mRNA Vaccines. *Mol Ther Nucleic Acids* **15**, 1-11, doi:10.1016/j.omtn.2019.01.013 (2019).

28   Gadde, S. *et al.* Development of therapeutic polymeric nanoparticles for the resolution of inflammation. *Adv Healthc Mater* **3**, 1448-1456, doi:10.1002/adhm.201300688 (2014).

29   Zhong, R. *et al.* Hydrogels for RNA delivery. *Nat Mater* **22**, 818-831, doi:10.1038/s41563-023-01472-w (2023).

30   Tang, X., Zhang, Y. & Han, X. Ionizable Lipid Nanoparticles for mRNA Delivery.

896   *Advanced NanoBiomed Research* **3**, 2300006, doi:10.1002/anbr.202300006 (2023).

897 31   Cui, K. *et al.* Epsin Nanotherapy Regulates Cholesterol Transport to Fortify Atheroma
898   Regression. *Circ Res* **132**, e22-e42, doi:10.1161/CIRCRESAHA.122.321723 (2023).

899 32   Gandara, C., Affleck, V. & Stoll, E. A. Manufacture of Third-Generation Lentivirus for
900   Preclinical Use, with Process Development Considerations for Translation to Good
901   Manufacturing Practice. *Hum Gene Ther Methods* **29**, 1-15, doi:10.1089/hgtb.2017.098
902   (2018).

903 33   Han, J. *et al.* Aberrant role of pyruvate kinase M2 in the regulation of gamma-secretase
904   and memory deficits in Alzheimer's disease. *Cell Rep* **37**, 110102,
905   doi:10.1016/j.celrep.2021.110102 (2021).

906 34   Liang, X. *et al.* A C-terminal glutamine recognition mechanism revealed by E3 ligase
907   TRIM7 structures. *Nat Chem Biol* **18**, 1214-1223, doi:10.1038/s41589-022-01128-x
908   (2022).

909 35   Almanza, A. *et al.* Regulated IRE1alpha-dependent decay (RIDD)-mediated
910   reprograming of lipid metabolism in cancer. *Nat Commun* **13**, 2493, doi:10.1038/s41467-
911   022-30159-0 (2022).

912 36   Comeau, S. R., Gatchell, D. W., Vajda, S. & Camacho, C. J. ClusPro: a fully automated
913   algorithm for protein-protein docking. *Nucleic Acids Res* **32**, W96-99,
914   doi:10.1093/nar/gkh354 (2004).

915 37   Comeau, S. R., Gatchell, D. W., Vajda, S. & Camacho, C. J. ClusPro: an automated
916   docking and discrimination method for the prediction of protein complexes.
917   *Bioinformatics* **20**, 45-50, doi:10.1093/bioinformatics/btg371 (2004).

918 38   Reaven, P., Merat, S., Casanada, F., Sutphin, M. & Palinski, W. Effect of streptozotocin-
919   induced hyperglycemia on lipid profiles, formation of advanced glycation endproducts in
920   lesions, and extent of atherosclerosis in LDL receptor-deficient mice. *Arterioscler*
921   *Thromb Vasc Biol* **17**, 2250-2256, doi:10.1161/01.atv.17.10.2250 (1997).

922 39   Balli, D., Zhang, Y., Snyder, J., Kalinichenko, V. V. & Kalin, T. V. Endothelial cell-
923   specific deletion of transcription factor FoxM1 increases urethane-induced lung
924   carcinogenesis. *Cancer Res* **71**, 40-50, doi:10.1158/0008-5472.CAN-10-2004 (2011).

925 40   Kim, I. M. *et al.* The forkhead box m1 transcription factor is essential for embryonic
926   development of pulmonary vasculature. *J Biol Chem* **280**, 22278-22286,
927   doi:10.1074/jbc.M500936200 (2005).

928 41   Sandelin, A., Alkema, W., Engstrom, P., Wasserman, W. W. & Lenhard, B. JASPAR: an
929   open-access database for eukaryotic transcription factor binding profiles. *Nucleic Acids*
930   *Res* **32**, D91-94, doi:10.1093/nar/gkh012 (2004).

931 42   Vlieghe, D. *et al.* A new generation of JASPAR, the open-access repository for
932   transcription factor binding site profiles. *Nucleic Acids Res* **34**, D95-97,
933   doi:10.1093/nar/gkj115 (2006).

934 43   Zhao, Y. Y. *et al.* Endothelial cell-restricted disruption of FoxM1 impairs endothelial
935   repair following LPS-induced vascular injury. *J Clin Invest* **116**, 2333-2343,
936   doi:10.1172/JCI27154 (2006).

937 44 Zhao, Y. D. *et al.* Endothelial FoxM1 mediates bone marrow progenitor cell-induced
938 vascular repair and resolution of inflammation following inflammatory lung injury. *Stem*
939 *Cells* **32**, 1855-1864, doi:10.1002/stem.1690 (2014).
940 45 Mirza, M. K. *et al.* FoxM1 regulates re-annealing of endothelial adherens junctions
941 through transcriptional control of beta-catenin expression. *J Exp Med* **207**, 1675-1685,
942 doi:10.1084/jem.20091857 (2010).
943 46 Huang, X. *et al.* Endothelial FoxM1 reactivates aging-impaired endothelial regeneration
944 for vascular repair and resolution of inflammatory lung injury. *Sci Transl Med* **15**,
945 eabm5755, doi:10.1126/scitranslmed.abm5755 (2023).
946 47 Gormally, M. V. *et al.* Suppression of the FOXM1 transcriptional programme via novel
947 small molecule inhibition. *Nat Commun* **5**, 5165, doi:10.1038/ncomms6165 (2014).
948 48 Wang, S. P. *et al.* FDI-6 inhibits the expression and function of FOXM1 to sensitize
949 BRCA-proficient triple-negative breast cancer cells to Olaparib by regulating cell cycle
950 progression and DNA damage repair. *Cell Death Dis* **12**, 1138, doi:10.1038/s41419-021-
951 04434-9 (2021).
952 49 Cheong, S. M., Choi, H., Hong, B. S., Gho, Y. S. & Han, J. K. Dab2 is pivotal for
953 endothelial cell migration by mediating VEGF expression in cancer cells. *Exp Cell Res*
954 **318**, 550-557, doi:10.1016/j.yexcr.2012.01.013 (2012).
955 50 Cheong, S. M., Choi, S. C. & Han, J. K. Xenopus Dab2 is required for embryonic
956 angiogenesis. *BMC Dev Biol* **6**, 63, doi:10.1186/1471-213X-6-63 (2006).
957 51 Fu, L. *et al.* Dab2 is a key regulator of endocytosis and post-endocytic trafficking of the
958 cystic fibrosis transmembrane conductance regulator. *Biochem J* **441**, 633-643,
959 doi:10.1042/BJ20111566 (2012).
960 52 Goren, I., Muller, E., Pfeilschifter, J. & Frank, S. Severely impaired insulin signaling in
961 chronic wounds of diabetic ob/ob mice: a potential role of tumor necrosis factor-alpha.
962 *Am J Pathol* **168**, 765-777, doi:10.2353/ajpath.2006.050293 (2006).
963 53 Kim, J. D. *et al.* Context-dependent proangiogenic function of bone morphogenetic
964 protein signaling is mediated by disabled homolog 2. *Dev Cell* **23**, 441-448,
965 doi:10.1016/j.devcel.2012.07.007 (2012).
966 54 Kim, J. D., Lee, H. W. & Jin, S. W. Diversity is in my veins: role of bone morphogenetic
967 protein signaling during venous morphogenesis in zebrafish illustrates the heterogeneity
968 within endothelial cells. *Arterioscler Thromb Vasc Biol* **34**, 1838-1845,
969 doi:10.1161/ATVBAHA.114.303219 (2014).
970 55 Li, Y. P. *et al.* Genetic polymorphism of the Dab2 gene and its association with Type 2
971 Diabetes Mellitus in the Chinese Uyghur population. *PeerJ* **11**, e15536,
972 doi:10.7717/peerj.15536 (2023).
973 56 Orlandini, M. *et al.* Morphogenesis of human endothelial cells is inhibited by DAB2 via
974 Src. *FEBS Lett* **582**, 2542-2548, doi:10.1016/j.febslet.2008.06.025 (2008).
975 57 Mishra, S. K. *et al.* Disabled-2 exhibits the properties of a cargo-selective endocytic
976 clathrin adaptor. *EMBO J* **21**, 4915-4926, doi:10.1093/emboj/cdf487 (2002).
977 58 Cheung, K. K., Mok, S. C., Rezaie, P. & Chan, W. Y. Dynamic expression of Dab2 in the

978 mouse embryonic central nervous system. *BMC Dev Biol* **8**, 76, doi:10.1186/1471-213X-
979 8-76 (2008).
980 59 Segarra, M. *et al.* Endothelial Dab1 signaling orchestrates neuro-glia-vessel
981 communication in the central nervous system. *Science* **361**, doi:10.1126/science.aao2861
982 (2018).
983 60 Adamson, S. E. *et al.* Deficiency of Dab2 (Disabled Homolog 2) in Myeloid Cells
984 Exacerbates Inflammation in Liver and Atherosclerotic Plaques in LDLR (Low-Density
985 Lipoprotein Receptor)-Null Mice-Brief Report. *Arterioscler Thromb Vasc Biol* **38**, 1020-
986 1029, doi:10.1161/ATVBAHA.117.310467 (2018).
987 61 Zha, W. *et al.* Efficient delivery of VEGF-A mRNA for promoting diabetic wound
988 healing via ionizable lipid nanoparticles. *Int J Pharm* **632**, 122565,
989 doi:10.1016/j.ijpharm.2022.122565 (2023).
990 62 Zhao, B. *et al.* Role of transcription factor FOXM1 in diabetes and its complications
991 (Review). *Int J Mol Med* **52**, doi:10.3892/ijmm.2023.5304 (2023).
992 63 Shirakawa, J. *et al.* Insulin Signaling Regulates the FoxM1/PLK1/CENP-A Pathway to
993 Promote Adaptive Pancreatic beta Cell Proliferation. *Cell Metab* **25**, 868-882 e865,
994 doi:10.1016/j.cmet.2017.02.004 (2017).

995